

Filament Plots for Data Visualization

Nate Strawn

NATE.STRAWN@GEORGETOWN.EDU

Department of Mathematics and Statistics

Georgetown University

Washington, D.C. 20037, USA

Editor:

Abstract

We construct a computationally inexpensive 3D extension of Andrew’s plots by considering curves generated by Frenet-Serret equations and induced by optimally smooth 2D Andrew’s plots. We consider linear isometries from a Euclidean data space to infinite dimensional spaces of 2D curves, and parametrize the linear isometries that produce (on average) optimally smooth curves over a given dataset. This set of optimal isometries admits many degrees of freedom, and (using recent results on generalized Gauss sums) we identify a particular a member of this set which admits an asymptotic projective “tour” property. Finally, we consider the unit-length 3D curves (filaments) induced by these 2D Andrew’s plots, where the linear isometry property preserves distances as “relative total square curvatures”. This work concludes by illustrating filament plots¹ for several datasets.

Keywords: Andrew’s plots, Gauss sums, Frenet-Serret, data visualization

1. Introduction

Data visualization is an essential component of data science, and scatter plots provide a primitive for many advanced visualization techniques. 2D scatter plots formed from d -dimensional data must generally compromise distances or similarities between d -dimensional data points. If a dataset $\{x_n\}_{n=1}^N \subset \mathbb{R}^d$ is mapped to \mathbb{R}^2 ($x_n \mapsto \Phi(x_n)$) with *distortion constant* $\eta \geq 1$, then

$$\eta^{-1} \|\Phi(x_n) - \Phi(x_m)\| \leq \|x_n - x_m\| \leq \eta \|\Phi(x_n) - \Phi(x_m)\| \text{ for all } n, m \in [N],$$

where $\|\cdot\|$ denotes Euclidean norms and $[N] = \{1, 2, \dots, N\}$ is the N -set. Here, the lower bound indicates that proximity in the data space implies proximity in the scatter plot, and the upper bound indicates that proximity in the scatter plot implies proximity in the data space.

Linear maps from \mathbb{R}^d to \mathbb{R}^2 produce severe distortion in general, so many non-linear embedding methods have been introduced to obtain better distortion constants. Multi-dimensional scaling (Kruskal, 1978) attempts to optimize embeddings of datasets to preserve distances on average, stochastic neighborhood embedding (t-SNE) (Van der Maaten and Hinton, 2008) seeks to preserve similarities according to a probabilistic model, (Brand and Huang, 2003) indicates that spectral embedding methods preserve angles, and UMAP

1. Code available at <https://github.com/n8epi/filaments>

(McInnes et al., 2018) applies category theory, fuzzy logic, and Laplacian eigenmaps to provide approximations to manifolds. Despite the flexibility provided by these methods, they still distort Euclidean distances when the dimension d and the number of samples N is large.

Other approaches simply consider complete preservation of information for each data point from the dataset. These methods trade visual complexity for data fidelity by merging multiple scatter plots from various projections. These methods include matrix of scatterplots (also known as pairs plots or draftsman’s plot) (Hartigan, 1975; Emerson et al., 2013; Tukey and Tukey, 1981), parallel coordinates plots/radar charts (Inselberg, 1985; Von Mayr, 1877), Andrew’s plots (Andrews, 1972), projection pursuit (Friedman and Tukey, 1974), and tours (Asimov, 1985). The first three methods yield “static” visualizations that are fixed for all time, and tours provide “dynamic” visualizations that consist of “movies” of scatterplots.

Matrix of scatterplots. An example is provided by Figure 1 for the iris dataset (Anderson, 1936). Matrix of scatterplots visualizations seemingly retain all information about the dataset, but suffer from an identifiability problem between points in each of the individual scatter plots. This becomes a severe issue when we consider dozens of dimensions since information about a single data point is scattered across the visualization. In fact, the pieces of visual information pertinent to a particular data point are spread uniformly throughout the plot as the dimension increases. Matrix of scatterplots visualizations also introduce bias by only considering a small sample of projections.

Parallel coordinates. Parallel coordinates plots (Figure 2) and radar charts solve the connectivity issue of matrix of scatterplots, but the interpolation approach to identifying individual data points produces high frequency visual clutter. This aesthetic unpleasantness also lead to practical difficulties in discerning relationships between variables or clusters of data points. While (Chen et al., 2011) considers a procedure for ordering parallel coordinates to minimize these aesthetic issues, the resulting plots are still difficult to read. Second, the graphs are lines in 2D laid on top of each other, so it is hard to parse differences as then number of graphs grows. While small multiples visualizations (Tufte et al., 1990) offer a partial remedy, they lose the ability to compare a multitude of points in a localized way.

Projection pursuit and tours. Grand tours Asimov (1985) are “smooth” movies of scatter plots as a projection varies over a Stiefel manifold. This provides an extreme remedy to the bias produced in the matrix of scatterplots visualizations. This strength leads to two weaknesses: the volume of information overwhelms the viewer and the “dynamic” nature of the visualization forces the viewer to rely on visual memory and tracking to discern patterns.

Projection pursuit (Friedman and Tukey, 1974) solves the issue of overwhelming information from the grand tour by selecting “interesting” projections of the data. (Cook et al., 1995) discusses how to integrate this with the grand tour to obtain visualizations. However, this method is still “dynamic” as well as computationally intensive.

1.1 Andrew’s plots

Andrew’s plots partially resolve the aesthetic issues for parallel coordinates plots, but may sacrifice the visibility of individual coordinates. Andrew’s plots originally consider mappings

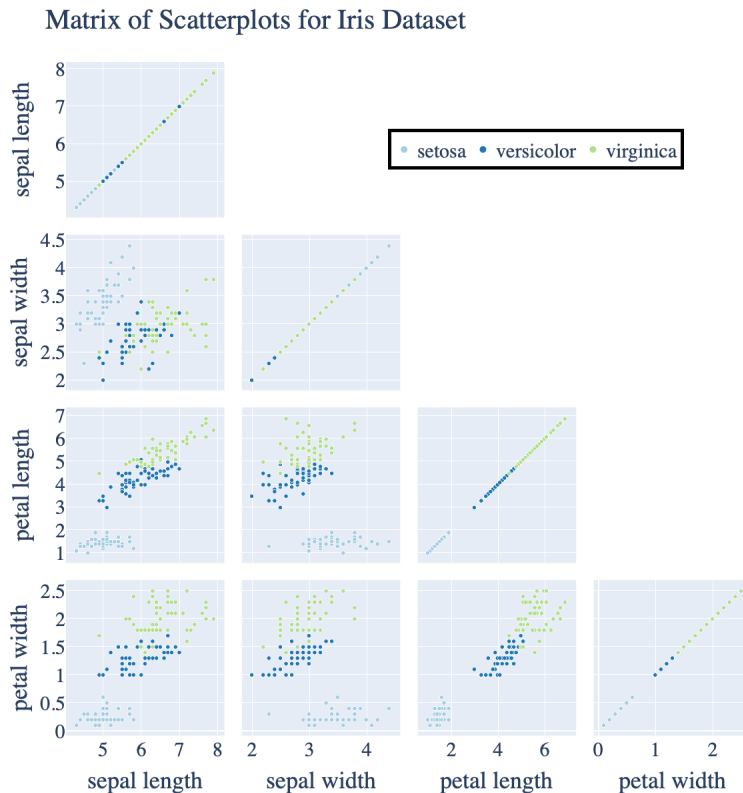


Figure 1: Matrix of scatterplots for the iris dataset.

of the form $\Phi : \mathbb{R}^d \rightarrow L^2([0, 1])$ satisfying

$$\Phi[x](t) = x_1 + x_2 \cos(2\pi t) + x_3 \sin(2\pi t) + x_4 \cos(4\pi t) + x_5 \sin(4\pi t) + \dots$$

That is, $\Phi[x]$ is a finite Fourier series using the lowest d frequencies. (Andrews, 1972) justifies using principal component scores instead of the original x_j 's by indicating that "low frequencies are more readily seen". Note that all of the principal components are used, so the plots are a lossless representation of the original dataset. Figure 4 illustrates Andrew's plots after standard transformations of the dataset.

Since Andrew's original paper, many authors introduced variations and interpretations of Andrew's plots. A recent perspective on Andrew's plot is given in (Moustafa, 2011). (Khattree and Naik, 2002) reviews several different ways to combine sin and cos functions, as well as various choices for frequency multipliers. (Wegman and Shen, 1993) consider multivariate Andrew's plots. Embrechts and Herzberg (1991) considers variations of Andrew's plots involving basis functions beyond the Fourier basis. Several papers consider extending Andrew's plots to map data points to parametric surfaces. (Koziol and Hacke, 1991) considers the case where data comes in pairs and a provides surface embeddings from this framework. (Garcia-Osorio and Fyfe, 2004, 2005) consider visualizations resulting from slices of 3D graphs of bivariate functions related to Andrew's plots.

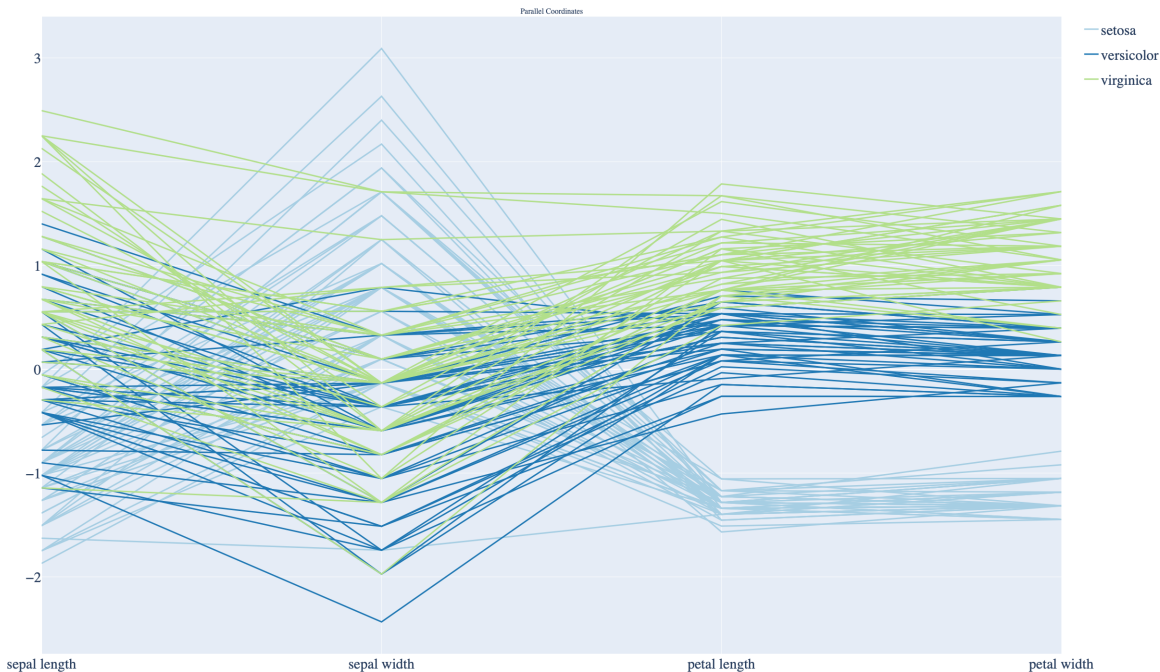


Figure 2: Parallel coordinates plot for the iris dataset.

(Wegman and Shen, 1993) creates a fast approximate grand tour structure by exploiting orthogonality – however this projective property does not maintain the full orthogonality property of the basis functions in each variable, so there are redundancies in the components of the curves. Their system is

$$\Phi(t) = \sqrt{\frac{2}{d}} \begin{pmatrix} \sin(\lambda_1 t) & \cos(\lambda_1 t) & \cdots & \sin(\lambda_{d/2} t) & \cos(\lambda_{d/2} t) \\ \cos(\lambda_1 t) & -\sin(\lambda_1 t) & \cdots & \cos(\lambda_{d/2} t) & -\sin(\lambda_{d/2} t) \end{pmatrix}$$

where $\lambda_1, \dots, \lambda_{d/2}$ are linearly independent over the rationals. This also sacrifices the isometry property. Instead, a “long term average” isometry property holds. Garcia-Osorio and Fyfe (2005) notes that this is related to a basis in derivatives of periodic curves, and observe that the system of projections encourages clusters to exhibit “flocking” behavior that data clusters may exhibit.

As indicated in Andrew’s original paper, the plots constitute a *linear isometry* from \mathbb{R}^d to $L^2([0, 1])$. That is, $\Phi[ax + by] = a\Phi[x] + b\Phi[y]$ for all $x, y \in \mathbb{R}^d$ and $a, b \in \mathbb{R}$, and

$$\|\Phi[x - y]\|_{L^2} = \|x - y\| \text{ for all } x, y \in \mathbb{R}^d.$$

Here, $\|\cdot\|_{L^2}$ is the standard L^2 norm on $L^2([0, 1])$, and we see that Andrew’s plots preserve Euclidean distances without distortion in the L^2 metric. This isometry property follows because the Fourier basis constitutes an orthonormal basis of $L^2([0, 1])$. This means that, unlike scatter plots in \mathbb{R}^2 , Andrew’s plots ensure that proximity in the visualization space implies proximity in the data space.

Unfortunately, L^2 distances between functions are not visually intuitive. One may view $\pi\|f\|_{L^2}^2$ as a volume of revolution, or an experienced electrical engineer may be able to

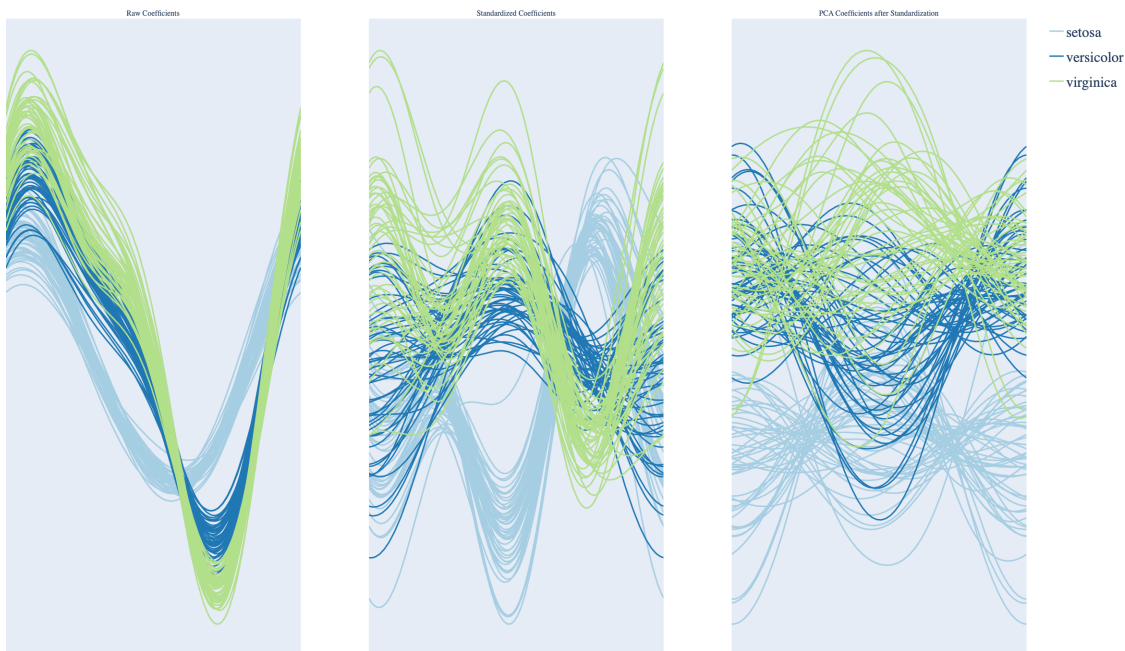


Figure 3: Andrew’s plots for the Iris dataset. The left plot provides the Andrew’s plot for the raw coefficients from the dataset, the center plot provides the Andrew’s plot after the coefficients are standardized, and the right plot uses the PCA scores after standardization.

understand $\|f\|_{L^2}^2$ as the energy of a voltage signal, but in general this quantity is not intuitive for most graphs of functions. On the other hand, the standard bounds

$$\|\Phi[x - y]\|_{L^1} \leq \|\Phi[x - y]\|_{L^2} \leq \|\Phi[x - y]\|_{L^\infty}$$

indicate that the net area between the Andrew’s plots is a lower bound, and the maximum absolute difference between the curves is an upper bound for the distance between x and y when Φ is a linear isometry. This upper bound is visually intuitive because we may just form a uniform band around an Andrew’s plot to obtain a neighborhood. The lower bound presents a greater challenge because areas present challenges to intuition.

Despite numerous variations on Andrew’s original idea, they still exhibit an issue with clutter; graphs are 1D curves plotted in 2D, so overlapping obscures information as the number of data points increases. Brushing techniques (Becker and Cleveland, 1987) are sometimes used to overcome this by highlighting collections of curves, but this technique may be applied to any visualization.

1.2 Ideal properties of 2D Andrew’s plots

In order to provide better spatial separation of curves for visualization, we consider graphs of 2D curves plotted in 3D, which may be examined in a “drag to rotate” interface. Ideally, these curves also retain all the desirable properties of Andrew’s plots:

1. The map from the Euclidean data space to $(L^2([0, 1]))^2$ is a linear isometry.

2. The linear isometry takes data to smooth curves.
3. The linear isometry property has accessible visual interpretations.
4. Displaying the curves is computationally inexpensive.

Subtle issues arise when we attempt to maintain these properties for 2D curves. We now identify five important properties that ensure visual appeal. By combining these properties, we obtain a constrained optimization problem over an infinite dimensional space of linear transformations.

Global non-degeneracy of curves and isometric isometries. First, a map of the form

$$\Phi[x](t) = \begin{pmatrix} x_1 + x_2\sqrt{2}\cos(2\pi t) + x_3\sqrt{2}\sin(2\pi t) + \dots \\ 0 \end{pmatrix}$$

is a linear isometry, but the plots of the resulting curves are confined to a two dimensional subspace of \mathbb{R}^3 , which obviates the reason for considering 2D curves in the first place. To restrict this type of degenerate behavior, we introduce the *isotropic isometry* condition for a linear map $\Phi : \mathbb{R}^d \rightarrow (L^2([0, 1]))^3$: for any $u \in \mathbb{R}^2$ with $\|u\| = 1$,

$$\|u^T \Phi[x]\|_{L^2} = \|x\| \text{ for all } x \in \mathbb{R}^d.$$

That is, for any unit vector $u \in \mathbb{R}^2$, the projection $x \mapsto u^T \Phi[x]$ is an isometry from \mathbb{R}^d to $L^2([0, 1])$.

Local non-degeneracy of curves and the projective tour property. While the isometric isometry condition prevents “global” degeneracies of curves, it is desirable to also prevent a “local” degeneracy of the curves as well. Suppose the linear map $\Phi(t) : \mathbb{R}^d \rightarrow \mathbb{R}^2$ has rank 1 for all $t \in [0, 1]$. Then there is a $\phi \in (L^2([0, 1]))^2$ such that (a) $\|\phi(t)\| = 1$ for all $t \in [0, 1]$, and (b) for each $x \in \mathbb{R}^d$ there is a $\gamma_x \in L^2([0, 1])$ with $\Phi[x](t) = \gamma_x(t)\phi(t)$ for almost all t . On the other hand, if $\Phi(t)$ has rank 2 for all $t \in [0, 1]$, then there are functions $\phi_1, \phi_2 \in (L^2([0, 1]))^2$ such that (a) $\phi_1(t), \phi_2(t) \subset \mathbb{R}^3$ is an orthonormal collection for each $t \in [0, 1]$ and (b) for each $x \in \mathbb{R}^d$ there are functions $\gamma_{x,1}, \gamma_{x,2} \subset L^2([0, 1])$ with

$$\Phi[x](t) = \gamma_1(t)\phi_1(t) + \gamma_2(t)\phi_2(t) \text{ for almost all } t \in [0, 1].$$

In the rank 1 case, we see that $\|\Phi[x] - \Phi[y]\|_{L^2}$ is mediated by only a single function $\gamma_x - \gamma_y$, whereas this difference is mediated by two functions $\{\gamma_{x,k} - \gamma_{y,k}\}_{k=1}^2$ in the rank 2 case. This means that the rank 2 case allows curves to diverge along as many directions as possible as the curves evolve in the plane. Therefore, to encourage this diverse directional divergence behavior, our final criteria is that Φ approximates a projective tour: there exists a $c > 0$ such that $c\Phi(t)$ is a rank 2 projection for all $t \in [0, 1]$.

Smooth curves and mean quadratic variation. The set of isotropic isometries $\Phi : \mathbb{R}^d \rightarrow (L^2([0, 1]))^2$ is vast, and a generic choice of Φ from this set produces noisy, high-frequency curves. To ensure the production of smooth curves, we choose Φ which minimizes the *mean quadratic variation*

$$\text{MQV}(\Phi, X) = \frac{1}{N} \sum_{n=1}^N \left\| \frac{d\Phi[x_n]}{dt} \right\|_{L^2}^2$$

where $X = (x_1 \ x_2 \ \cdots \ x_N) \in \mathbb{R}^{d \times N}$ is a data matrix for a dataset $\{x_j\}_{j=1}^N \subset \mathbb{R}^d$, and $\|\cdot\|_{L^2}$ is an L^2 norm for vector-valued functions over $[0, 1]$:

$$\left\| \frac{d\Phi[x_n]}{dt} \right\|_{L^2}^2 = \int_0^1 \left\| \frac{d\Phi[x_n]}{dt}(t) \right\|^2 dt.$$

By minimizing the mean quadratic variation over a dataset, we force the curves to exhibit some degree of smoothness.

Interpretability of isometries for spaces of derivatives. Finally, we consider the interpretation of the L^1 and L^∞ bounds in the context of these 2D curves. While the L^∞ bound is relatively easy to interpret, the L^1 bound is not visually intuitive. However, if we assume that the isometry Φ takes data to *derivatives* of smooth curves, then the L^1 bound describes the lengths of curves and the L^∞ bound applies to the instantaneous velocities of curves.

Removal of visual bias and closed curves. Integrals of 2D space curves may be separated into affine and periodic components:

$$\gamma(t) = ct + \tilde{\gamma}(t)$$

where $c \in \mathbb{R}^2$, and $\tilde{\gamma}(0) = \tilde{\gamma}(1)$. A linear isometry from \mathbb{R}^d to $(L^2([0, 1]))^2$ induces a linear isometry to the coefficients of the affine component of these maps. Inclusion of the affine components creates a visual impact dominated by information equivalent to two scatterplots, which is necessarily lossless. To avoid this visual bias, we restrict the images of isometries to periodic functions on $[0, 1]$.

1.3 Summary of main results

While combining the isometric isometry property and the projective tour property while minimizing the mean quadratic variation presents a substantial computational challenge, it is possible to characterize the minimizers which satisfy the isometric isometry property and extract such a minimizer that satisfies an approximate tour property. Here, we summarize our main results.

1. We parameterize the set of minimizers of the mean quadratic variation subject to the isotropic isometry condition (Theorem 4).
2. In general, the set of minimizers has d degrees of freedom, and we exhibit a particular choice of minimizer that admits a projective tour property in an asymptotic sense (Theorem 6).

It should be noted that one may reformulate the proof of Theorem 4 to demonstrate that PCA scores provide Andrew’s plots that minimize the mean quadratic variation over a dataset subject to an isometry condition. Figure 4 illustrates the resulting plots for the iris dataset.

When plotting the resulting graphs of curves, we observe clutter due to the fact that the tangents to the graphs always agree on the first component. To declutter the 3D plots,

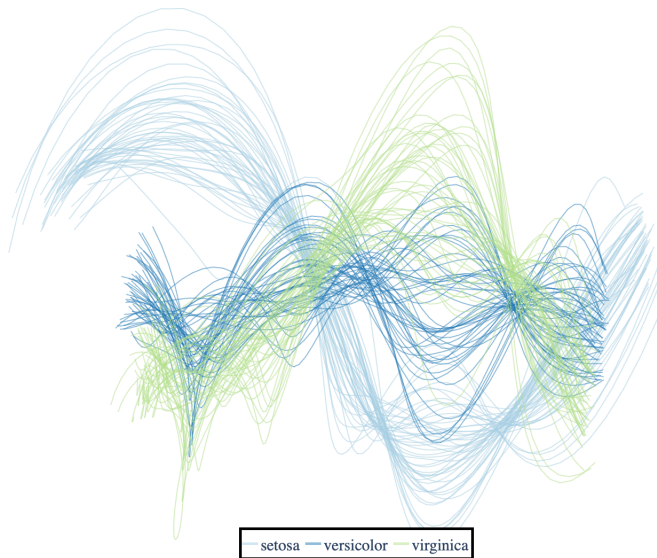


Figure 4: The graphs of the 2D Andrew’s plots for the iris dataset.

we consider mapping from $(L^2([0, 1]))^2$ to the space of arc-length parameterized curves in \mathbb{R}^3 with total length 1 by imposing the condition that the derivative of the tangent of this curve satisfies

$$d\mathbf{T}(t) = \kappa_1(t)\mathbf{N}_1(t) + \kappa_2(t)\mathbf{N}_2(t)$$

where $\mathbf{T}, \mathbf{N}_1, \mathbf{N}_2$ constitute a moving frame determined by the functions $\kappa_1, \kappa_2 \in L^2([0, 1])$. Therefore, our \mathbb{R}^2 curves give rise to \mathbb{R}^3 curves, and we also show that the isometry condition may be interpreted in terms of “relative” curvatures. This interpretation follows from the fact that a curve satisfying the above formula has the curvature function $\kappa(t) = \sqrt{\kappa_1^2(t) + \kappa_2^2(t)}$. While the resulting curves now involve a non-linear transformation of the data that exhibits anisotropic evolution of data curves, the resulting plots are still interesting and computationally efficient to produce. These filament plots are illustrated in Figure 5.

1.4 Organization of this paper

Section 2 introduces definitions and theory to establish the technical setting for our main results. Section 2 provides the full statements of Theorem 4 and Theorem 6. Section 3 provides the proof of Theorem 4, Section 4 establishes the proof of Theorem 6, and Section 5 describes the non-linear procedure for producing space curves via a moving frame and Frenet-Serret type equations. Sections 3 and 4 both conclude by discussing related technical results and ideas. Section 5 concludes with visualizations of the iris dataset, Boston housing dataset, Wisconsin breast cancer dataset, and a dataset of handwritten digits. Section 6 concludes the paper with a discussion of interesting ramifications and potential future directions.

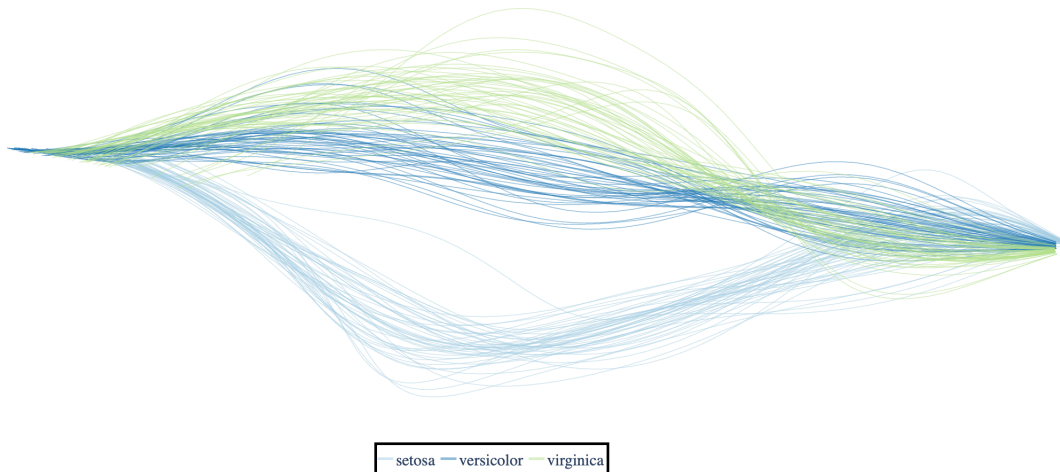


Figure 5: The Filament plot for the iris dataset.

2. Main results

Our results hold over spaces of square integrable functions. Let $L^2([0, 1])$ denote the Hilbert space of square integrable (in the Lebesgue sense) functions with norm $\|\cdot\|_{L^2}$ and inner product $\langle \cdot, \cdot \rangle_{L^2}$, and set

$$\mathcal{H}^1([0, 1]) = \left\{ f \in L^2([0, 1]) : \frac{df}{dt} \text{ is defined almost everywhere, } \frac{df}{dt} \in L^2([0, 1]) \right\}$$

In other words, $\mathcal{H}^1([0, 1])$ is the Sobolev space of square integrable functions over $[0, 1]$ with square integrable derivatives over $[0, 1]$. Since the decorations of $\mathcal{H}^1([0, 1])$ never change, we simply write \mathcal{H} for the remainder of the paper.

We define the space $\mathcal{H}^d \subset (L^2([0, 1]))^d$ so that $\phi \in \mathcal{H}^d$ if and only if $\phi : [0, 1] \rightarrow \mathbb{R}^d$ has component functions $\phi_k \in \mathcal{H}$ for $k = 1, \dots, d$. Note that \mathcal{H}^d inherits the (incomplete) norm

$$\|\phi\|_{L^2} = \sqrt{\int_0^1 \|\phi(t)\|^2 dt}$$

from $(L^2([0, 1]))^d$, where $\|\cdot\|$ is the standard Euclidean norm on \mathbb{R}^d .

We define the space $\mathcal{H}^{2 \times d} \subset (L^2([0, 1]))^{2 \times d}$ so that $\Phi \in \mathcal{H}^{2 \times d}$ if and only if $\Phi : [0, 1] \rightarrow \mathbb{R}^{2 \times d}$ has component functions $\phi_{j,k} \in \mathcal{H}$ for all $j = 1, 2$ and $k = 1, \dots, d$. Here $\mathbb{R}^{2 \times d}$ denotes the space of all 2 by d matrices with real entries. Note that $\mathcal{H}^{2 \times d}$ inherits the norm

$$\|\Phi\|_{L^2} = \sqrt{\int_0^1 \|\Phi(t)\|^2 dt}$$

from $(L^2([0, 1]))^{2 \times d}$, where

$$\|A\| = \sqrt{\text{trace}(A^T A)}$$

is the Frobenius norm of a matrix $A \in \mathbb{R}^{2 \times d}$.

For $\Phi \in \mathcal{H}^{2 \times d}$, we call the $\phi_{j,\cdot}^T \in \mathcal{H}^d$ functions the *component slices* of Φ , we call the 2 by d matrices $\Phi(t)$ the *time slices* of Φ , and we call the functions $\phi_{\cdot,k} \in \mathcal{H}^2$ the *coordinate slices* of Φ . Figure 6 illustrates the time slices of such a tensor.

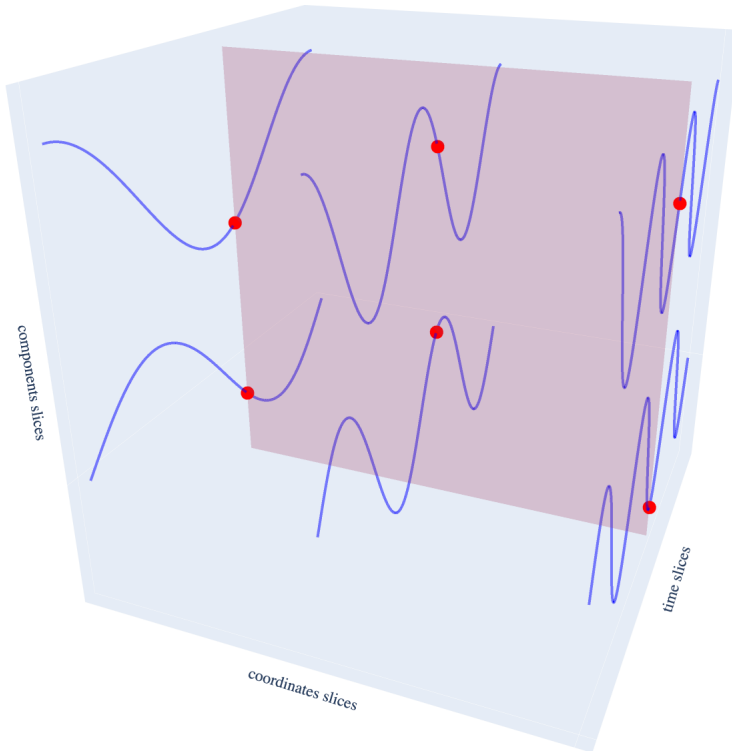


Figure 6: An example of “false” time slices for $\Phi \in \mathcal{H}^{2 \times 3}$. Here there are two possible component slices, three possible coordinate slices, and a continuum of time slices. The “entries” of a time slice $\Phi(t)$ are illustrated by the red markers.

Consider the set of all linear operators $\mathcal{L}(\mathbb{R}^d, \mathcal{H}^2)$. These are all bounded (and hence continuous) since the unit ball of \mathbb{R}^d is compact. Just as linear functions between Euclidean spaces are related to matrices, members of $\mathcal{L}(\mathbb{R}^d, \mathcal{H}^2)$ may be characterized by matrix-valued functions whose entries are characterized by the next proposition.

Proposition 1 $\Omega \in \mathcal{L}(\mathbb{R}^d, \mathcal{H}^2)$ is linear if and only if there is a $\Phi \in \mathcal{H}^{2 \times d}$ such that $\Omega[x](t) = \Phi(t)x$ for all $x \in \mathbb{R}^d$ and almost all $t \in [0, 1]$.

The proof of this proposition is a simple exercise, so we omit it. Based on Proposition 1, we abuse notation by allowing $\Phi[x]$ to denote the operator induced by $\Phi \in \mathcal{H}^{2 \times d}$ applied to the vector $x \in \mathbb{R}^d$. We define the *quadratic variation* of $f \in \mathcal{H}^2$ by

$$\text{QV}(f) = \int_0^1 \left\| \frac{df}{dt}(t) \right\|^2 dt.$$

For a dataset $X = \{x_n\}_{n=1}^N \subset \mathbb{R}^d$ and a mapping $\Phi \in \mathcal{H}^{2 \times d}$ the mean quadratic variation is

$$\text{MQV}(\Phi; X) = \frac{1}{N} \sum_{n=1}^N \text{QV}(\Phi[x_n]).$$

This measures the average “smoothness” of the Φ mapping over the dataset. The next proposition simplifies the structure of the isotropic isometry condition for such a Φ .

Proposition 2 $\Phi \in \mathcal{L}(\mathbb{R}^d, \mathcal{H}^2)$ is an isotropic isometry if and only if

$$\int_0^1 \phi_{j,k}(t) \phi_{j',k'}(t) dt = \delta_{(j,k),(j',k')}$$

for all $(j,k), (j',k') \in [2] \times [d]$, where $[2] = \{1, 2\}$, $[d] = \{1, \dots, d\}$, and $\delta_{(k,j),(k',j')}$ is a Kronecker delta function.

In other words, the entry functions of the matrix-valued function Φ form an orthonormal collection in $L^2([0, 1])$. The proof of the difficult implication in this proposition is a straightforward application of the parallelogram identity, so we omit it.

We additionally impose the constraint that

$$\int_0^1 \Phi[x](t) dt = 0 \text{ for all } x \in \mathbb{R}^d.$$

This constraint implies Φ maps into spaces of discrete derivatives of closed curves. The conditions

$$\int_0^1 \phi_{j,k}(t) dt = 0 \text{ for all } j \in [2], k \in [d]$$

encode this constraint. Combining this constraint with the isometry constraint means that Φ is a norm-preserving map onto spaces of derivatives of closed curves. Therefore, Φ induces a map onto spaces of functions such that the norm-difference in the data space is analogous to the energy-difference of the path.

We now define the set $\mathcal{S}^{2,d}(X)$ that shall ultimately constitute the minimizers of our constrained optimization program. For a matrix $A \in \mathbb{R}^{2 \times k}$, we define the *vectorization operator* $\alpha : \mathbb{R}^{2 \times k} \rightarrow \mathbb{R}^{2k}$ by

$$\alpha \begin{pmatrix} a_{1,1} & a_{1,2} & \cdots & a_{1,k} \\ a_{2,1} & a_{2,2} & \cdots & a_{2,k} \end{pmatrix} = \begin{pmatrix} a_{1,1} \\ a_{1,2} \\ \vdots \\ a_{1,k} \\ a_{2,1} \\ a_{2,2} \\ \vdots \\ a_{2,k} \end{pmatrix}, \text{ and note that } \alpha^{-1} \begin{pmatrix} x \\ y \end{pmatrix} = \begin{pmatrix} x^T \\ y^T \end{pmatrix}.$$

for all $x, y \in \mathbb{R}^k$. Using this vectorization operator, we define a group action of $\mathcal{O}(2k)$ on $\mathcal{H}^{2 \times k}$ so that $U \in \mathcal{O}(2k)$ and $\Psi \in \mathcal{H}^{2 \times k}$, then $U \cdot \Psi \in \mathcal{H}^{2 \times k}$ is defined by

$$(U \cdot \Psi)(t) = \alpha^{-1}(U \alpha(\Psi(t))) \text{ for almost all } t \in [0, 1].$$

We define the functions $c_k, s_k \in \mathcal{H}$ by $c_k(t) = \sqrt{2} \cos(2\pi kt)$ and $s_k(t) = \sqrt{2} \sin(2\pi kt)$ (note that $\sqrt{2}$ is the normalization constant). For $k_1, k_2 \in [d]$ satisfying $k_1 \leq k_2$, we let $\Pi_{[k_1, k_2]}$ denote the orbit of

$$\Psi_{k_1, k_2}(t) = \begin{pmatrix} c_{k_1}(t) & \cdots & c_{k_2}(t) \\ s_{k_1}(t) & \cdots & s_{k_2}(t) \end{pmatrix}$$

under this action by $\mathcal{O}(2(k_2 - k_1 + 1))$. We note that $\Psi \in \Pi_{[k_1, k_2]}$ if and only if the component functions of Ψ form an orthonormal basis of

$$\text{span}\{c_{k_1}, \dots, c_{k_2}, s_{k_1}, \dots, s_{k_2}\} \subset L^2([0, 1]).$$

When $k \in [d]$, we simply write $\Pi_k = \Pi_{[k, k]}$ and note that Π_k is the orbit of the curve $(c_k \ s_k)^T \in \mathcal{H}^2$ under the left-multiplication action of $\mathcal{O}(2)$.

Let $X \in \mathbb{R}^{d \times N}$, suppose $X = U\Sigma V^T$ is a singular value decomposition of X , and that the partition $\{[k_{q, \min}, k_{q, \max}]\}_{q=1}^p$ of $[d]$ satisfies

$$\sigma_k = \sigma_{k_{q, \min}} \text{ if and only if } k \in [k_{q, \min}, k_{q, \max}].$$

Definition 3 *Suppose $X \in \mathbb{R}^{d \times N}$ has the SVD $X = U\Sigma V^T$. Then $\Phi \in \mathcal{S}^{2,d}(X)$ if and only if $\tilde{\Phi}(t) = \Phi(t)U$ satisfies*

$$\tilde{\Phi}_{[k_{q, \min}, k_{q, \max}]} = \begin{pmatrix} \tilde{\phi}_{1, k_{q, \min}} & \cdots & \tilde{\phi}_{1, k_{q, \max}} \\ \tilde{\phi}_{2, k_{q, \min}} & \cdots & \tilde{\phi}_{2, k_{q, \max}} \end{pmatrix} \in \Pi_{[k_{q, \min}, k_{q, \max}]}$$

for all $q \in [p]$.

Our optimization program is

$$\min_{\Phi \in \mathcal{H}^{2 \times d}} \text{MQV}(\Phi; X) \tag{1}$$

subject to the constraints

$$\int_0^1 \phi_{k,j}(t) \phi_{k',j'}(t) dt = \delta_{(k,j), (k',j')}.$$

for all $(k, j), (k', j') \in [2] \times [d]$ and

$$\int_0^1 \phi_{k,j}(t) dt = 0.$$

for all $(k, j) \in [2] \times [d]$. We are now in a position to state our main result.

Theorem 4 *The system $\Phi \in \mathcal{L}(\mathbb{R}^d, \mathcal{H}^2)$ solves Program 1 if and only if $\Phi \in \mathcal{S}^{2,d}(X)$.*

This theorem completely specifies the degrees of freedom for the solutions to the minimization problem. The following corollary considers the simplification when the singular values of X are distinct.

Corollary 5 *If the $X = U\Sigma V^T \in \mathbb{R}^{d \times N}$ has distinct singular values, then $\Phi \in \mathcal{S}^{2,d}(X)$ if and only if there is a collection $\{Q_k\}_{k=1}^d \subset \mathcal{O}(2)$ such that $\tilde{\Phi} = \Phi \cdot U$ has coordinate slices*

$$\tilde{\phi}_{\cdot,k} = Q_k \begin{pmatrix} c_k \\ s_k \end{pmatrix}$$

Example 1 *Figure 6 illustrates the matrix-valued function*

$$\Psi(t) = \begin{pmatrix} c_1(t) & c_2(t) & c_3(t) \\ s_1(t) & s_2(t) & s_3(t) \end{pmatrix}.$$

Given a data matrix $X \in \mathbb{R}^{3 \times N}$ with distinct singular values and an SVD $X = U\Sigma V^T$, then Φ is a minimizer of Program 1 if and only if there are 2 by 2 rotation matrices Q_1 , Q_2 , and Q_3 such that

$$\Phi(t) = \left(Q_1 \begin{pmatrix} c_1(t) \\ s_1(t) \end{pmatrix} \quad Q_2 \begin{pmatrix} c_2(t) \\ s_2(t) \end{pmatrix} \quad Q_3 \begin{pmatrix} c_3(t) \\ s_3(t) \end{pmatrix} \right) U^T$$

for almost all $t \in [0, 1]$.

In the generic case, $X = U\Sigma V^T$ has distinct singular values and $\mathcal{S}^{2 \times d}(X)$ is invariant under the action of $\mathcal{O}(2)^d$ that applies to each column after multiplication by U^T . We now exploit these degrees of freedom to push the time slices $\Phi(t)$ towards projections to obtain an approximate tour property. We let

$$U(s) = \begin{pmatrix} \cos(2\pi s) & -\sin(2\pi s) \\ \sin(2\pi s) & \cos(2\pi s) \end{pmatrix}$$

Theorem 6 *Fix $\Phi \in \mathcal{S}^{2 \times d}(I_d)$ by specifying $U_k = U(k^2/4d)$ for $k \in [d]$ and setting*

$$\phi_{\cdot,k} = U_k \begin{pmatrix} c_k \\ s_k \end{pmatrix} \text{ for all } k \in [d]$$

Then the scaled time slices $\sqrt{\frac{1}{d}}\Phi(t)$ all have singular values in the interval

$$\left[\sqrt{1 - \left(\frac{4}{\sqrt{d}} + \frac{2}{d} + \frac{2}{d^2} \right)}, \sqrt{1 + \left(\frac{4}{\sqrt{d}} + \frac{2}{d} + \frac{2}{d^2} \right)} \right].$$

for all $t \in [0, 1]$.

Example 2 *Figure 7 illustrates the behavior of the singular values of*

$$\frac{1}{2}\Psi(t) = \frac{1}{\sqrt{2}} \begin{pmatrix} \cos(2\pi t) & \cos(4\pi t) & \cos(6\pi t) & \cos(8\pi t) \\ \sin(2\pi t) & \sin(4\pi t) & \sin(6\pi t) & \sin(8\pi t) \end{pmatrix}$$

and $\Phi(t)$ obtained through quadratic phase shifts of the columns of Ψ suggested by Theorem 6.

We note that (Khattree and Naik, 2002) is obliquely related to this choice (for 1D Andrew's plots). Their suggested basis consists rotations of the orthogonal pairs corresponding to a rotation by $e^{\pi i/2}$, so one can envision how this might "unroll" to a \mathbb{R}^2 example. However, this will still have degenerate projections near $t = 1/2$.

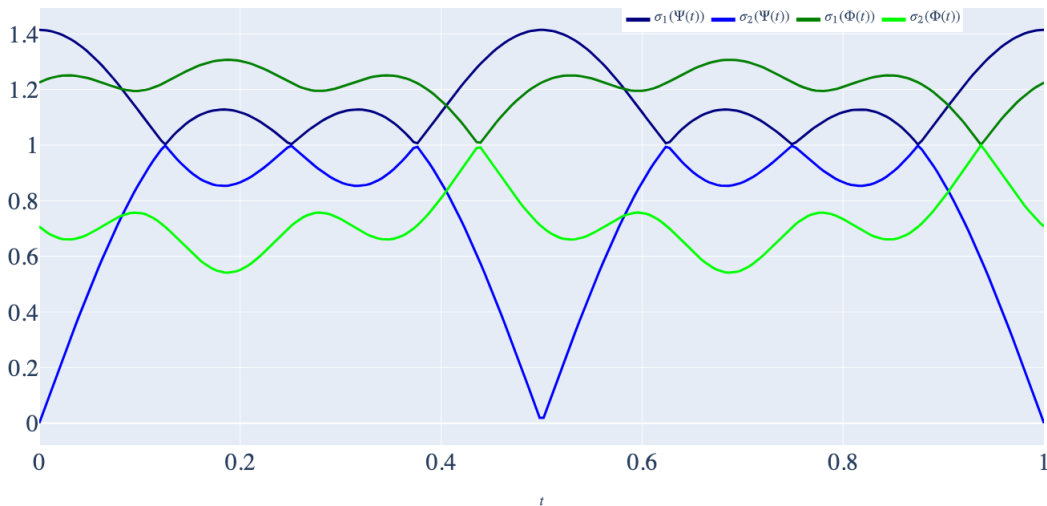


Figure 7: Singular values before and after quadratic phase shifts for minimizers Ψ and Φ from Theorem 4 with $d = 4$.

3. Minimizers of the MQV and $\mathcal{S}^{2,d}(X)$

This section provides a proof for Theorem 4. The proof exploits the vector-valued Fourier transform. Because we use closed curves, we have $\Phi[x] \in (L^2([0, 1]))^2$ has the vector-valued Fourier representation

$$\Phi[x](t) = \sum_{k \in \mathbb{Z}} \widehat{\Phi[x]}(k) e^{2\pi i k t}$$

where $\widehat{\Phi[x]}(k) \in \mathbb{C}^2$ and $\widehat{\Phi[x]}(-k) = \overline{\widehat{\Phi[x]}(k)}$ since our curves are real-valued.

For the next lemma, we define the Stiefel manifold $\text{St}(d, M)$ to be the set of all matrices $V \in \mathbb{C}^{d \times M}$ such that $VV^* = I_d$

Lemma 7 *Suppose $0 \leq \lambda_1 \leq \lambda_2 \leq \dots \leq \lambda_M$, set $D = \text{diag}(\lambda_1, \lambda_2, \dots, \lambda_M) \in \mathbb{R}^{M \times M}$. Then*

$$\sum_{k=1}^d \lambda_k = \min_{V \in \text{St}(d, M)} \text{trace}(VDV^*)$$

and $VDV^* = \sum_{k=1}^d \lambda_k$ if and only if there is a $Q \in \mathcal{U}(d)$ such that the rows of Q^*V are an orthonormal collection of eigenvectors corresponding to the eigenvalues $\lambda_1, \dots, \lambda_d$.

Proof The lower bound follows from the Courant-Fischer min-max theorem. To obtain the optimality characterization, note that the constraints are regular, and hence the Lagrange conditions become

$$VD = \Lambda V \text{ and } VV^* = I_d$$

for some Hermitian matrix of Lagrange multipliers $\Lambda \in \mathbb{R}^{d \times d}$. Since Λ is Hermitian, it is diagonalizable, and in particular there is a unitary matrix $Q \in \mathcal{U}(d)$ such that $\Lambda = Q\Theta Q^*$ where Θ is a diagonal matrix with non-increasing diagonal entries. Then

$$Q^*VD = \Theta Q^*V.$$

Therefore the rows of $Q^T V$ form eigenvectors of D with eigenvalues θ_k . Moreover, $Q^* V (Q^* V)^* = I_d$ gives that these eigenvectors are orthonormal. Finally,

$$\text{trace}(VDV^*) = \text{trace}(\Lambda VV^*) = \text{trace}(\Lambda) = \sum_{k=1}^d \theta_k$$

so eigenvalues $\{\theta_k\}_{k=1}^d$ must match with the eigenvalues $\{\lambda_k\}_{k=1}^d$ to ensure equality for the lower bound. \blacksquare

This lemma allows us to precisely characterize the degrees of freedom of solutions to trace optimization problems subject to orthonormality constraints.

Lemma 8 *Suppose $X \in \mathbb{R}^{d \times N}$ has the singular value decomposition $X = U \Sigma V^T$. For $\Phi \in \mathcal{H}^{2 \times d}$, define $\tilde{\Phi} \in \mathcal{H}^{2 \times d}$ by setting $\tilde{\Phi}(t) = \Phi(t) U^T$, and set*

$$h_{j,k} = \left\| \frac{d\tilde{\phi}_{j,k}}{dt} \right\|_{L^2}^2$$

for all $j \in [2]$ and $k \in [d]$. Then

$$\text{MQV}(\Phi; X) = \sum_{k=1}^{d-1} (\sigma_k^2 - \sigma_{k+1}^2) \sum_{l=1}^k (h_{1,l} + h_{2,l}) + \sigma_d^2 \sum_{k=1}^d (h_{1,k} + h_{2,k})$$

Proof For any $x \in \mathbb{R}^d$, linearity of integration and matrix multiplication yield

$$\begin{aligned} \text{QV}(\Phi[x]) &= \int_0^1 \left\| \frac{d\Phi[x]}{dt}(t) \right\|^2 dt \\ &= \int_0^1 \left[\left(\frac{d\phi_{1,\cdot}}{dt}(t)x \right)^2 + \left(\frac{d\phi_{2,\cdot}}{dt}(t)x \right)^2 \right] dt \\ &= \int_0^1 \left[x^T \left(\frac{d\phi_{1,\cdot}}{dt}(t) \right)^T \frac{d\phi_{1,\cdot}}{dt}(t)x + x^T \left(\frac{d\phi_{2,\cdot}}{dt}(t) \right)^T \frac{d\phi_{2,\cdot}}{dt}(t)x \right] dt \\ &= x^T \left(\int_0^1 \left(\frac{d\phi_{1,\cdot}}{dt}(t) \right)^T \frac{d\phi_{1,\cdot}}{dt}(t) dt \right) x + x^T \left(\int_0^1 \left(\frac{d\phi_{2,\cdot}}{dt}(t) \right)^T \frac{d\phi_{2,\cdot}}{dt}(t) dt \right) x \end{aligned}$$

Setting

$$G_{j,j'}(\Phi) = \int_0^1 \left(\frac{d\phi_{j,\cdot}}{dt}(t) \right)^T \frac{d\phi_{j',\cdot}}{dt}(t) dt \text{ for } j, j' \in [2] \quad (2)$$

we have

$$\begin{aligned} \text{QV}(\Phi[x]) &= x^T G_{1,1}(\Phi)x + x^T G_{2,2}(\Phi)x \\ &= \text{trace} \left[\begin{pmatrix} xx^T & 0 \\ 0 & xx^T \end{pmatrix} \begin{pmatrix} G_{1,1}(\Phi) & 0 \\ 0 & G_{2,2}(\Phi) \end{pmatrix} \right]. \end{aligned}$$

From this expression, it follows that

$$\text{MQV}(\Phi; x) = \frac{1}{N} \text{trace} \left[\begin{pmatrix} XX^T & 0 \\ 0 & XX^T \end{pmatrix} \begin{pmatrix} G_{1,1}(\Phi) & 0 \\ 0 & G_{2,2}(\Phi) \end{pmatrix} \right]$$

Setting $\Lambda = \Sigma\Sigma^T$, note that $U^T G_{j,j}(\Phi)U = G_{j,j}(\tilde{\Phi})$, and so invariance of the trace under conjugation by U gives

$$\begin{aligned} \text{MQV}(\Phi; X) &= \frac{1}{N} \text{trace} \left[\begin{pmatrix} \Lambda & 0 \\ 0 & \Lambda \end{pmatrix} \begin{pmatrix} G_{1,1}(\tilde{\Phi}) & 0 \\ 0 & G_{2,2}(\tilde{\Phi}) \end{pmatrix} \right] \\ &= \sigma_1^2 h_{1,1} + \sigma_1^2 h_{2,1} + \dots + \sigma_d^2 h_{1,d} + \sigma_d^2 h_{2,d} \end{aligned}$$

where the last line follows because $\Lambda = \text{diag}(\sigma_1^2, \dots, \sigma_d^2)$ and $\text{diag}(G_{j,j}(\tilde{\Phi})) = (h_{j,1} \ h_{j,2} \ \dots \ h_{j,d})^T$ for $j \in [2]$. The Abel summation formula yields

$$\begin{aligned} \text{MQV}(\Phi; X) &= (\sigma_1^2 - \sigma_2^2)(h_{1,1} + h_{2,1}) \\ &\quad + (\sigma_2^2 - \sigma_3^2)(h_{1,1} + h_{2,1} + h_{1,2} + h_{2,2}) \\ &\quad + \dots \\ &\quad + (\sigma_{d-1}^2 - \sigma_d^2) \left(\sum_{k=1}^{d-1} (h_{1,k} + h_{2,k}) \right) + \sigma_d^2 \sum_{k=1}^d (h_{1,k} + h_{2,k}) \end{aligned}$$

and the result is complete. ■

Lemma 9 *Suppose d and N are natural numbers with $d \leq N$ and let $X \in \mathbb{R}^{d \times N}$ have a singular value decomposition $X = U\Sigma V^T$. For all $\Phi \in \mathcal{H}^{2 \times d}$, satisfying*

$$\langle \phi_{j,k}, \phi_{j',k'} \rangle_{L^2} = \delta_{(j,k),(j',k')} \text{ for all } j, j' \in [2], k, k' \in [d]$$

and

$$\langle \phi_{j,k}, \mathbf{1}_{[0,1]} \rangle_{L^2} = 0 \text{ for all } j \in [2], k \in [d],$$

$$\text{MQV}(\Phi; X) \geq 2 \sum_{s=1}^{d-1} (\sigma_s^2 - \sigma_{s+1}^2) \sum_{k=1}^s k^2 + 2\sigma_d^2 \sum_{k=1}^d k^2 \quad (3)$$

Moreover, equality holds if and only if

$$\sum_{k=1}^s (h_{1,k} + h_{2,k}) = 2 \sum_{k=1}^s k^2$$

for all s such that $\sigma_s \neq \sigma_{s+1}$ or $s = d$, where $h_{j,k}$ is defined in the previous lemma.

Proof Since the σ_k 's form a non-increasing sequence, $\sigma_s - \sigma_{s+1} \geq 0$. Moreover, $h_{j,k} \geq 0$ for all $j \in [2]$ and $k \in [d]$, so the final statement follows by invoking the Lemma 8.

Without loss of generality, we assume $U = I$ so that $\tilde{\Phi} = \Phi$ from the previous lemma. We define the block matrix

$$G = \begin{pmatrix} G_{1,1}(\Phi) & G_{1,2}(\Phi) \\ G_{2,1}(\Phi) & G_{2,2}(\Phi) \end{pmatrix}$$

where $G_{j,j'}(\Phi)$ is defined by equation (2), and we define the submatrices

$$G^{(s)} = \begin{pmatrix} G_{1,1}(\Phi) & G_{1,2}(\Phi) \\ G_{2,1}(\Phi) & G_{2,2}(\Phi) \end{pmatrix}$$

where $G_{j,j'}^{(s)}(\Phi)$ is the s by s submatrix in the upper left corner of $G_{j,j'}(\Phi)$ for $j, j' \in [2]$.

Since $\phi_{j,k} \in \mathcal{H}$, $\phi_{j,k}$ admits a Fourier transform $\hat{\phi}_{j,k}$. The condition $\int_0^1 \phi_{j,k}(t) dt = 0$ is equivalent to $\hat{\phi}_{j,k}(0) = 0$. Moreover, Parseval-Plancherel provides

$$[G_{j,j'}(\Phi)]_{k,k'} = \left\langle \frac{d\phi_{j,k}}{dt}, \frac{d\phi_{j',k'}}{dt} \right\rangle_{L^2} = \sum_{m \in \mathbb{Z}} m^2 \hat{\phi}_{j,k}(m) \overline{\hat{\phi}_{j',k'}(m)}$$

For all natural numbers M , we set

$$\hat{\Phi}_{s,M} = \begin{pmatrix} \hat{\phi}_{1,1}(-M) & \hat{\phi}_{1,1}(-M+1) & \cdots & \hat{\phi}_{1,1}(-1) & \hat{\phi}_{1,1}(1) & \cdots & \hat{\phi}_{1,1}(M-1) & \hat{\phi}_{1,1}(M) \\ \vdots & \vdots & \ddots & \vdots & \vdots & \ddots & \vdots & \vdots \\ \hat{\phi}_{1,s}(-M) & \hat{\phi}_{1,s}(-M+1) & \cdots & \hat{\phi}_{1,s}(-1) & \hat{\phi}_{1,s}(1) & \cdots & \hat{\phi}_{1,s}(M-1) & \hat{\phi}_{1,s}(M) \\ \hat{\phi}_{2,1}(-M) & \hat{\phi}_{2,1}(-M+1) & \cdots & \hat{\phi}_{2,1}(-1) & \hat{\phi}_{2,1}(1) & \cdots & \hat{\phi}_{2,1}(M-1) & \hat{\phi}_{2,1}(M) \\ \vdots & \vdots & \ddots & \vdots & \vdots & \ddots & \vdots & \vdots \\ \hat{\phi}_{2,s}(-M) & \hat{\phi}_{2,s}(-M+1) & \cdots & \hat{\phi}_{2,s}(-1) & \hat{\phi}_{2,s}(1) & \cdots & \hat{\phi}_{2,s}(M-1) & \hat{\phi}_{2,s}(M) \end{pmatrix}$$

so that $\hat{\Phi}_{s,M} \in \mathbb{C}^{2d \times 2M}$, and fix the diagonal matrix

$$\mathcal{Q}_{s,M} = \begin{pmatrix} (s+1)^2 I_{M-s+1} & 0 & 0 \\ 0 & \mathcal{Q}_s & 0 \\ 0 & 0 & (s+1)^2 I_{M-s+1} \end{pmatrix}$$

for all $M > s$ where

$$\mathcal{Q}_s = \text{diag}(s^2, (s-1)^2, \dots, 1, 1, \dots, (s-1)^2, s^2).$$

Note that $\hat{\Phi}_{s,M} \mathcal{Q}_{s,M} \hat{\Phi}_{s,M}$ converges to some matrix $H^{(s)}$ as $M \rightarrow \infty$ since

$$\lim_{M \rightarrow \infty} \hat{\Phi}_{s,M} \mathcal{Q}_{s,M} \hat{\Phi}_{s,M} \rightarrow G^{(s)}.$$

In particular

$$\lim_{M \rightarrow \infty} \sum_{|m| \leq s} m^2 |\hat{\phi}_{1,1}(m)|^2 + (s+1)^2 \sum_{s < |m| \leq s} m^2 |\hat{\phi}_{1,1}(m)|^2 = H_{1,1}^{(s)} \text{ for all } s \in [d],$$

and

$$1 = \|\phi_{1,1}\|_{L^2}^2 = \sum_{m \in \mathbb{Z}} |\hat{\phi}_{1,1}(m)|^2$$

implies $\|H^{(s)}\| > 0$ for all $s \in [d]$. Therefore, there is an M_0 such that $M \geq M_0$ implies

$$\|\hat{\Phi}_{s,M} \mathcal{Q}_{s,M} \hat{\Phi}_{s,M} - H^{(s)}\| \leq \|H^{(s)}\|.$$

This establishes the bound

$$\|\hat{\Phi}_{s,M} \mathcal{Q}_{s,M} \hat{\Phi}_{s,M}\| \leq 2\|H^{(s)}\| \text{ for all } M \geq M_0. \quad (4)$$

Let $\varepsilon > 0$, and set

$$\varepsilon' = \left(\frac{\varepsilon}{2\sqrt{2s}\|H^{(s)}(\Phi)\| + \varepsilon} \right) \wedge \frac{1}{2}$$

Observing that $\lim_{M \rightarrow \infty} \hat{\Phi}_{s,M} \hat{\Phi}_{s,M}^* = I_{2s}$, let M' be so large that $M \geq M'$ implies

$$\|\hat{\Phi}_{s,M} \hat{\Phi}_{s,M}^* - I_{2s}\| < \varepsilon'.$$

This implies that the eigenvalues of $\hat{\Phi}_{s,M} \hat{\Phi}_{s,M}^*$ are bounded below by $\frac{1}{2} \leq 1 - \varepsilon'$. Thus, $\hat{\Phi}_{s,M} \hat{\Phi}_{s,M}^*$ is invertible for all $M \geq M'$. Moreover, the eigenvalues of $\hat{\Phi}_{s,M} \hat{\Phi}_{s,M}^*$ satisfy

$$|1 - \nu_k^{-1}| \leq \frac{\varepsilon'}{1 - \varepsilon'} \text{ for all } M \geq M'$$

Taking the square root sum of squares we get

$$\left\| I_{2s} - (\hat{\Phi}_{s,M} \hat{\Phi}_{s,M}^*)^{-1} \right\| \leq \sqrt{2s} \frac{\varepsilon'}{1 - \varepsilon'} \leq \frac{\varepsilon}{2\|H^{(s)}\|}. \quad (5)$$

Also note that $V_{s,M} = (\hat{\Phi}_{s,M} \hat{\Phi}_{s,M}^*)^{-1/2} \hat{\Phi}_{s,M}$ has orthonormal rows for $M \geq M'$.

Then (with $h_{j,k}$ defined in the previous lemma),

$$\begin{aligned} & \sum_{k=1}^s (h_{1,k} + h_{2,k}) \\ &= \sum_{k=1}^s \sum_{m \in \mathbb{Z}} m^2 (|\hat{\phi}_{1,k}(m)|^2 + |\hat{\phi}_{2,k}(m)|^2) \\ &\geq \sum_{k=1}^s \left[\sum_{|m| \leq s} m^2 (|\hat{\phi}_{1,k}(m)|^2 + |\hat{\phi}_{2,k}(m)|^2) + (s+1)^2 \sum_{s < |m|} (|\hat{\phi}_{1,k}(m)|^2 + |\hat{\phi}_{2,k}(m)|^2) \right] \end{aligned} \quad (6)$$

$$\geq \sum_{k=1}^s \left[\sum_{|m| \leq s} m^2 (|\hat{\phi}_{1,k}(m)|^2 + |\hat{\phi}_{2,k}(m)|^2) + (s+1)^2 \sum_{\substack{s < |m| \\ |m| \leq M}} (|\hat{\phi}_{1,k}(m)|^2 + |\hat{\phi}_{2,k}(m)|^2) \right] \quad (7)$$

$$= \text{trace} \left(\hat{\Phi}_{s,M} \mathcal{Q}_{s,M} \hat{\Phi}_{s,M}^* \right) - \text{trace} \left(V_{s,M} \mathcal{Q}_{s,M} V_{s,M}^* \right) + \text{trace} \left(V_{s,M} \mathcal{Q}_{s,M} V_{s,M}^* \right)$$

$$= \text{trace} \left(V_{s,M} \mathcal{Q}_{s,M} V_{s,M}^* \right) + \text{trace} \left(\left(I_{2s} - (\hat{\Phi}_{s,M} \hat{\Phi}_{s,M}^*)^{-1} \right) \hat{\Phi}_{s,M} \mathcal{Q}_{s,M} \hat{\Phi}_{s,M}^* \right)$$

Now note that

$$\left\| \hat{\Phi}_{s,M} \mathcal{Q}_{s,M} \hat{\Phi}_{s,M}^* \right\| \leq 2 \|H^{(s)}(\Phi)\|$$

And Cauchy-Schwarz on the Hilbert-Schmidt inner product yields

$$\begin{aligned} \sum_{k=1}^s (\delta_{1,k} + \delta_{2,k}) &\geq \text{trace} (V_{s,M} \mathcal{Q}_{s,M} V_{s,M}^*) - \left\| I_{2s} - (\hat{\Phi}_{s,M} \hat{\Phi}_{s,M}^*)^{-1} \right\| \left\| \hat{\Phi}_{s,M} \mathcal{Q}_{s,M} \hat{\Phi}_{s,M}^* \right\| \\ &\geq \text{trace} (V_{s,M} \mathcal{Q}_{s,M} V_{s,M}^*) - \varepsilon. \end{aligned}$$

This last bound follows from the inequalities (4) and (5) as long as $M > \max(s, M_0, M')$.

By applying Lemma 7 to $\mathcal{Q}_{s,M}$ and $V_{s,M}$,

$$\text{trace} (V_{s,M} \mathcal{Q}_{s,M} V_{s,M}^*) \geq \sum_{k=1}^s 2k^2,$$

and we conclude that

$$\begin{aligned} &\sum_{k=1}^s \left[\sum_{|m| \leq s} m^2 (|\hat{\phi}_{1,k}(m)|^2 + |\hat{\phi}_{2,k}(m)|^2) + (s+1)^2 \sum_{s < |m|} (|\hat{\phi}_{1,k}(m)|^2 + |\hat{\phi}_{2,k}(m)|^2) \right] \\ &\geq \left(\sum_{k=1}^s 2k^2 \right) - \varepsilon. \end{aligned}$$

Since $\varepsilon > 0$ was arbitrary, the approximation property of inequalities yields

$$\sum_{k=1}^s \left[\sum_{|m| \leq s} m^2 (|\hat{\phi}_{1,k}(m)|^2 + |\hat{\phi}_{2,k}(m)|^2) + (s+1)^2 \sum_{s < |m|} (|\hat{\phi}_{1,k}(m)|^2 + |\hat{\phi}_{2,k}(m)|^2) \right] \geq \sum_{k=1}^s 2k^2. \quad (8)$$

Then the inequality (6) gives

$$\sum_{k=1}^s (h_{1,k} + h_{2,k}) \geq \left(\sum_{k=1}^s 2k^2 \right) - \varepsilon.$$

Since $\varepsilon > 0$ was arbitrary, we conclude the result. \blacksquare

Proof [Proof of Theorem 4] Without loss of generality, the singular value decomposition $X = U \Sigma V^T$ satisfies $U = I$, so $\tilde{\Phi}$ is just Φ .

We first note that, for all s such that $\sigma_s \neq \sigma_{s+1}$ or $s = d$, the system of equalities from Lemma 9

$$\sum_{k=1}^s (h_{1,k} + h_{2,k}) = 2 \sum_{k=1}^s k^2$$

is equivalent to the system of equalities

$$\sum_{k=k_{q,\min}}^{k_{q,\max}} (h_{1,k} + h_{2,k}) = 2 \sum_{k=k_{q,\min}}^{k_{q,\max}} k^2 \text{ for all } q \in [p].$$

First suppose that $\Phi_{[k_{q,\min}, k_{q,\max}]} \in \Pi_{[k_{q,\min}, k_{q,\max}]}$ for all $q \in [p]$. Then there is a $Q_q \in \mathcal{O}(2(k_{q,\max} - k_{q,\min} + 1))$ such that

$$Q_q^T \cdot \Phi_{[k_{q,\min}, k_{q,\max}]} = \Psi_{k_{q,\min}, k_{q,\max}}$$

because Q_q preserves norms, we have that

$$\sum_{k=k_{q,\min}}^{k_{q,\max}} (h_{1,k} + h_{2,k}) = \left\| \frac{d\Phi_{[k_{q,\min}, k_{q,\max}]}}{dt} \right\|_{L^2}^2 = \left\| \frac{d\Psi_{k_{q,\min}, k_{q,\max}}}{dt} \right\|_{L^2}^2 = 2 \sum_{k=k_{q,\min}}^{k_{q,\max}} k^2.$$

Thus, Φ is a minimizer by Lemma 9.

To prove the converse, we first note that if Φ has any component $\phi_{j,k}$ such that $\hat{\phi}_{j,k}$ does not have finite support, then the inequality (6) is strict for $s = d$, so Lemma 9 indicates that Φ cannot be a minimizer.

Thus, if Φ is a minimizer, then all of the sequences $\hat{\phi}_{j,k}$ have finite support, and hence there exists a natural number M such that $\hat{\Phi}_{s,M}$ from Lemma 9 satisfies

$$\text{trace} \left(\hat{\Phi}_{s,M} \mathcal{Q}_M \hat{\Phi}_{s,M}^* \right) = 2 \sum_{k=1}^s k^2,$$

and therefore Lemma 7 gives a $Q \in \mathcal{U}(2M)$ such that $Q^* \hat{\Phi}_{s,M}$ has orthonormal rows of eigenvectors of \mathcal{Q}_M corresponding to the lowest $2s$ eigenvalues of \mathcal{Q}_M . Consequently, we must have that $\Phi_{[1,s]} \in \Pi_{[1,s]}$ for $s = d$ and all s with $\sigma_s \neq \sigma_{s+1}$. Then $\Phi_{[k_{1,\min}, k_{1,\max}]}$ $\in \Pi_{[k_{1,\min}, k_{1,\max}]}$ and an induction argument establishes the result. ■

3.1 Discussion

We note that

$$\begin{aligned} \|\Phi[x](t)\| &\leq \sum_{k \in \mathbb{Z}} \left\| \widehat{\Phi[x]}(k) \right\| = \sum_{k \in \mathbb{Z}} \frac{1}{k} \left\| k \widehat{\Phi[x]}(k) \right\| \\ &\leq \sqrt{\sum_{k \in \mathbb{Z}} \frac{1}{k^2}} \sqrt{\sum_{k \in \mathbb{Z}} \left\| k \widehat{\Phi[x]}(k) \right\|^2} \\ &= C \left\| \frac{d\Phi[x]}{dt} \right\|_{L^2}, \end{aligned}$$

for all $t \in [0, 1]$, so $\|\Phi[x]\|_{L^\infty} \leq C \left\| \frac{d\Phi[x]}{dt} \right\|_{L^2}$ for all $x \in \mathbb{R}^d$. Thus, we have that minimization of the mean quadratic variation also squeezes the gap present in the bound

$$\|\Phi[x_j]\|_{L^1} \leq \|\Phi[x_j]\|_{L^2} \leq \|\Phi[x_j]\|_{L^\infty}.$$

The main theorem may be imitated for curves embedded in arbitrary dimension. However, different principal components are identified with similar frequencies for 1D curves,

and the assignment of the principal components in the \mathbb{R}^3 is staggered. The plots of such curves are still informative, but lack the symmetry enjoyed by the \mathbb{R}^2 embeddings. In particular, the \mathbb{R}^3 case does not generally enjoy the property that projections onto 1D subspaces of \mathbb{R}^2 result in the same 1D MQV.

This result may also be imitated for other quadratic forms, but now the result will identify PCA components to eigenfunctions of some other operator. For example, the Legendre basis arises from minimizing the discrete Legendre equations, and the Hermite functions come from the Schrodinger-Laplacian. This may have some relevance with respect to the work [Embrechts and Herzberg \(1991\)](#), but we do not explore this possibility here.

Theorem 4 also suggests that the optimal embeddings are related to partial Laurent series with a 0 constant component under the identification of \mathbb{R}^2 with \mathbb{C} .

4. Quadratic phase shifts and the asymptotic tour property

This section provides the proof of Theorem 6. We begin with a lemma reminiscent of Theorem 2.7 of ([Goyal et al., 2001](#)):

Lemma 10 *Suppose $Z = \{z_k\}_{i=k}^d \subset \mathbb{C}$ and $w \in \mathbb{C}$ satisfies*

$$\sum_{k=1}^d |z_k|^2 = 2 \text{ and } \sum_{k=1}^d z_k^2 = \omega^2,$$

and set $a_k = \text{Re}(z_k)$ and $b_k = \text{Im}(z_k)$ for $k \in [d]$. Then the singular values of the matrix

$$Z = \begin{pmatrix} a_1 & \cdots & a_d \\ b_1 & \cdots & b_d \end{pmatrix}$$

are $\sqrt{1 \pm \frac{|\omega|^2}{2}}$.

Proof We note that

$$A = ZZ^T = \begin{pmatrix} \sum_{k=1}^d a_k^2 & \sum_{k=1}^d a_k b_k \\ \sum_{k=1}^d a_k b_k & \sum_{k=1}^d b_k^2 \end{pmatrix}$$

has trace

$$\sum_{k=1}^d a_k^2 + \sum_{i=1}^d b_k^2 = \sum_{i=1}^d |z_k|^2 = 2.$$

Let $\omega = v + iw$, set

$$\widehat{Z} = \begin{pmatrix} a_1 & \cdots & a_d & -w \\ b_1 & \cdots & b_d & v \end{pmatrix}$$

and observe that

$$2\left(\sum_{k=1}^d a_k b_k - wv\right) = \text{Im}\left(\sum_{k=1}^d z_k^2 - \omega^2\right) = 0,$$

and

$$\sum_{k=1}^d a_k^2 + w^2 - \sum_{k=1}^d b_k^2 - v^2 = \text{Re}\left(\sum_{k=1}^d z_k^2 - \omega^2\right) = 0$$

so $\widehat{Z}\widehat{Z}^T$ is a diagonal matrix with a constant diagonal $c = \sum_{k=1}^d a_k^2 + w^2$. If $\omega = 0$, then $ZZ^T = \widehat{Z}\widehat{Z}^T$ and $\text{trace}(ZZ^T) = 2$ gives $ZZ^T = I_2$ and the result follows.

On the other hand, if $\omega \neq 0$, then

$$ZZ^T = \widehat{Z}\widehat{Z}^T - \begin{pmatrix} -w \\ v \end{pmatrix} \begin{pmatrix} -w \\ v \end{pmatrix}^T = cI_2 - \begin{pmatrix} -w \\ v \end{pmatrix} \begin{pmatrix} -w \\ v \end{pmatrix}^T,$$

the eigenvectors of ZZ^T are

$$\begin{pmatrix} w \\ w \end{pmatrix}, \begin{pmatrix} -w \\ v \end{pmatrix}$$

with eigenvalues c and $c - |\omega|^2$. Since $\text{trace}(ZZ^T) = 2$, $2 = 2c - |\omega|^2$, and we conclude that $c = \frac{1}{2} \frac{|\omega|^2}{1}$. This verifies that the eigenvalues of ZZ^T are $1 \pm \frac{|\omega|^2}{2}$ and expression for the singular values of Z follow. \blacksquare

Proof [Proof of Theorem 6] Let $t \in [0, 1]$ and set $z_k = (\phi_{1,k}(t) + i\phi_{2,k}(t))/\sqrt{2}$ for $k \in [d]$. Since

$$\begin{pmatrix} \phi_{1,k}(t) \\ \phi_{2,k}(t) \end{pmatrix} = \begin{pmatrix} \cos(\pi k^2/2d) & -\sin(\pi k^2/2d) \\ \sin(\pi k^2/2d) & \cos(\pi k^2/2d) \end{pmatrix} \begin{pmatrix} \sqrt{2} \cos(2\pi kt) \\ \sqrt{2} \sin(2\pi kt) \end{pmatrix},$$

it follows that $|z_k|^2 = 1$ for all $k \in [d]$, so $\sum_{k=1}^d |z_k|^2 = d$. Moreover, we see that

$$z_k = e^{2\pi i \frac{k^2}{4d}} e^{2\pi i kt}.$$

Then

$$\sum_{k=1}^d z_k^2 = \sum_{k=1}^d e^{\pi i \frac{k^2}{d}} e^{2\pi i k(2t)}.$$

noting that

$$e^{2\pi i k(2t)} = e^{2\pi i k(2t-1)} = e^{2\pi i k(2t-2)}$$

for all $k \in [d]$, this sum has the form

$$S_N(x, \theta) = \sum_{k=1}^N f(k)$$

where $f(k) = e^{\pi i x k^2} e^{2\pi i k \theta}$, $N = d$, $x = 1/d \in (0, 1)$, and $\theta \in [-1/2, 1/2]$. In the notation of (Paris, 2014), we let erfc denote the complementary error function defined by the line integral

$$\text{erfc}(z) = 1 - \text{erf}(z) = \frac{2}{\sqrt{\pi}} \int_{|z|}^{\infty} e^{-w^2} dw,$$

and set

$$E(\tau) = e^{-\pi i \tau^2/x} \text{erfc} \left(\omega \tau \sqrt{\pi/x} \right) = e^{-\pi i d \tau^2} \frac{2}{\sqrt{\pi}} \int_{\tau \sqrt{\pi/x}}^{\infty} e^{-is^2} ds,$$

where $\omega = e^{-\pi i/4}$. The paper (Paris, 2014) derives the expression

$$S_N(x, \theta) = \frac{1}{2}(f(N) - 1) + J_N + e^{\pi i/4}(I_N - I_0)$$

where

$$J_N = \frac{e^{\pi i/4}}{2\sqrt{x}} (E(\theta) - f(N)E(\xi)),$$

for $\xi = Nx + \theta$ and

$$I_j = \frac{f(j)}{2\sqrt{x}} \sum_{k=1}^{\infty} (E(k - jx - \theta) - E(k + jx + \theta))$$

for $j = 0, N$.

We have that $|\frac{1}{2}(f(N) - 1)| \leq 1$. Then using the substitution $s = u\sqrt{\pi/2}$ gives

$$\left| \int_{\tau\sqrt{\pi/x}}^{\infty} e^{is^2} ds \right| = \left| \int_{\tau\sqrt{2/x}}^{\infty} \cos(\pi u^2/2) du + i \int_{\tau\sqrt{2/x}}^{\infty} \sin(\pi u^2/2) du \right| \leq 2$$

and

$$|J_N| \leq \frac{2}{\sqrt{x}}$$

It remains to bound the expressions

$$I_j = \frac{f(j)}{2\sqrt{x}} \sum_{k=1}^{\infty} (E(k - jx - \theta) - E(k + jx + \theta))$$

for $j = 0, N$. Under our constraints, we only consider the sums

$$\sum_{k=1}^{\infty} E(k - \theta) - E(k + \theta)$$

and

$$\sum_{k=1}^{\infty} E(k - 1 - \theta) - E(k + 1 + \theta)$$

We note that $f(0) = 1$.

Using the asymptotic formulation in (Paris, 2014) (equation 2.2) which cites Olver et al. (2010) (error bound derivations are from Olver (1997)), we have (for $k \geq 1$),

$$E(k - \theta) - E(k + \theta) = \frac{\sqrt{x}}{\sqrt{\pi}} e^{\pi i/4} (k - \theta)^{-1} + R(k - \theta) - \frac{\sqrt{x}}{\sqrt{\pi}} e^{\pi i/4} (k + \theta)^{-1} - R(k + \theta)$$

which gives

$$E(k - \theta) - E(k + \theta) = \frac{\sqrt{x}}{\sqrt{\pi}} e^{\pi i/4} \frac{2\theta}{k^2 - \theta^2} + R$$

The bound for the remainder terms is given by

$$\frac{x^{3/2}}{2\pi^2} \left(\frac{1}{(k - \theta)^3} + \frac{1}{(k + \theta)^3} \right)$$

We have

$$\sum_{k=1}^{\infty} \frac{1}{k^2 - \theta^2} \leq \sum_{k=2}^{\infty} \frac{1}{k^2 - \frac{1}{4}} = 2,$$

so the first terms contribute at most

$$2\sqrt{\frac{x}{\pi}}.$$

On the other hand, the contribution of the inverse cubic terms is at most $9\frac{x^{3/2}}{\pi^2}$.

For the second series, we have a similar situation, the asymptotic formula for $E(1-1-\theta)$ may not hold, so now we must estimate the first term using the bound 4 Then the remaining terms satisfy

$$E(k-1-\theta) - E(k+1+\theta) = \frac{\sqrt{x}}{\sqrt{\pi}} e^{\pi i/4} (k-1-\theta)^{-1} + R(k-1-\theta) - \frac{\sqrt{x}}{\sqrt{\pi}} e^{\pi i/4} (k+1+\theta)^{-1} - R(k+1+\theta)$$

which gives

$$E(k-1-\theta) - E(k+1+\theta) = \frac{\sqrt{x}}{\sqrt{\pi}} e^{\pi i/4} \frac{2\theta}{k^2 - (1+\theta)^2} + R$$

The bound for the remainder terms is given by

$$\frac{x^{3/2}}{2\pi^2} \left(\frac{1}{(k-1-\theta)^3} + \frac{1}{(k+1+\theta)^3} \right)$$

The first part contributes at most

$$\frac{46}{45} \sqrt{\frac{x}{\pi}}$$

Because of the shift by 1, the remainder p -series contributes something on the same order. So, the total contribution of the I_j terms is

$$\frac{1}{2\sqrt{x}} \left(2\sqrt{\frac{x}{\pi}} + 9\frac{x^{3/2}}{\pi^2} + \frac{46}{45}\sqrt{\frac{x}{\pi}} + 4 + 9\frac{x^{3/2}}{\pi^2} \right) \leq 1 + 2x + \frac{2}{\sqrt{x}}$$

The final bound is

$$\frac{4}{\sqrt{x}} + 2 + 2x = 4\sqrt{d} + 2 + \frac{2}{d}.$$

Multiplying all z_i by the constant $\sqrt{\frac{2}{d}}$, we invoke the lemma to observe that $\sqrt{\frac{1}{d}}\Phi(t)$ has singular values between

$$\sqrt{1 \pm \left(\frac{4}{\sqrt{d}} + \frac{2}{d} + \frac{2}{d^2} \right)}.$$

Since t was arbitrary, we see that this bound holds for all t . ■

We note that this asymptotic rate for a uniform bound is optimal. This is because the expectation of the square magnitude satisfies

$$\int_0^1 \left| \sum_{k=1}^d \alpha_k e^{2\pi i k t} \right|^2 dt = \sum_{k=1}^d |\alpha_k|^2,$$

so the maximum value of magnitude is at least \sqrt{d} given $|\alpha_k| = 1$ for all $k \in [d]$.

4.1 Discussion of quadratic Gauss sums

The work from (Hardy et al., 1914) derives the basic bound for our expression, but (Paris, 2014) has a form amenable to expressing the bound explicitly for finite dimension. (Lehmer, 1976) considers incomplete Gauss sums which are related to our approach and has the right form for asymptotics. This paper also has a geometric interpretation of the cancellations in the sum, and cumulative generalized Gaussian sums form interesting spiral structures related to Euler spirals.

An elementary derivation of the quadratic Gauss sum is given in (Murty and Pathak, 2017), and it also details the resulting quadratic reciprocity result. The paper Oskolkov (1991) considers sums of the form required in this paper (generalized Gaussian sums), but the sums are infinite. The textbooks (Berndt et al., 1998; Iwaniec and Kowalski, 2004) derive expressions for generalized Gaussian sums, but the range of the coefficients is outside of our interest.

The work (Bourgain and Chang, 2006) establishes bounds for Gauss sums over additive characters of finite fields, and (Demirci Akarsu and Marklof, 2013) consider limit distributions of Gauss sums. (Coutsias and Kazarinoff, 1998) considers a precise bound for the “functional” approximation formula. This applies for the small $1/d$ in our case, but works in the continuous setting and excludes the linear terms we need.

5. Inducing 3D curves from Frenet-Serret equations

We now consider transporting a moving frame $\mathbf{T}, \mathbf{N}_1, \mathbf{N}_2$ of orthonormal vectors in \mathbb{R}^3 subject to the condition

$$\frac{d\mathbf{T}}{dt}(t) = \kappa_1(t)\mathbf{N}_1(t) + \kappa_2(t)\mathbf{N}_2(t).$$

Since the matrix

$$U(t) = \begin{pmatrix} \mathbf{T}(t) \\ \mathbf{N}_1(t) \\ \mathbf{N}_2(t) \end{pmatrix}$$

is orthogonal, the derivative must satisfy

$$\frac{dU}{dt}(t) = Z(t)U(t)$$

where $Z(t)$ is a skew-symmetric matrix. We then see that

$$Z(t) = \begin{pmatrix} 0 & \kappa_1(t) & \kappa_2(t) \\ -\kappa_1(t) & 0 & 0 \\ -\kappa_2(t) & 0 & 0 \end{pmatrix}$$

satisfies the desired properties. The additional degree of freedom represented by the 2, 3 entry of this matrix corresponds to infinitesimal rotation of \mathbf{N}_1 and \mathbf{N}_2 in their span, by excluding this term, we maintain a diversity of curves while ensuring a simple geometric interpretation of the mean quadratic variation.

By fiat, the curvature of the curve with tangent \mathbf{T} is $\kappa(t) = \sqrt{\kappa_1(t)^2 + \kappa_2(t)^2}$. Moreover, normal vector of the induced curve is

$$\mathbf{N}(t) = \frac{\kappa_1(t)}{\kappa(t)}\mathbf{N}_1(t) + \frac{\kappa_2(t)}{\kappa(t)}\mathbf{N}_2(t) = \cos(\theta(t))\mathbf{N}_1(t) + \sin(\theta(t))\mathbf{N}_2(t).$$

Here, we only assume θ is differentiable. Taking a cross product with \mathbf{T} , the binormal of the induced curve is (up to a sign determined by the orientation of the initial frame)

$$\mathbf{B}(t) = \sin(\theta(t))\mathbf{N}_1(t) - \cos(\theta(t))\mathbf{N}_2(t).$$

Taking derivatives, we get

$$\mathbf{B}'(t) = \theta'(t)\mathbf{N}(t) - [\sin(\theta(t))\kappa_1'(t) - \cos(\theta(t))\kappa_2'(t)]\mathbf{T}(t) = \theta'(t)\mathbf{N}(t),$$

so the torsion function satisfies $\tau(t) = \|\mathbf{B}'(t)\| = |\theta'(t)|$. So, the polar decomposition

$$\kappa_1(t) + i\kappa_2(t) = \kappa(t)e^{i\theta(t)},$$

relates κ_1 and κ_2 to the curvature and torsion of the induced curves. Thus, we have independent curvatures and torsion. Now, how does the derivative of the curvature impact the torsion? When we take the derivate of this expression, we have

$$\kappa_1'(t) + i\kappa_2'(t) = \kappa'(t)e^{i\theta(t)} + i\theta'(t)\kappa(t)e^{i\theta(t)}$$

so taking the absolute value gives us

$$|\kappa_1'(t) + i\kappa_2'(t)| = |\kappa'(t) + i\theta'(t)\kappa(t)|$$

and the square provides

$$\kappa_1'(t)^2 + \kappa_2'(t)^2 = \kappa'(t)^2 + \theta'(t)^2\kappa(t)^2$$

Therefore, minimization of the mean quadratic variation of κ_1 and κ_2 is equivalent to minimizing the sum of the mean quadratic variation of the curvature function and the L^2 inner product of the squared torsion function with the squared curvature function. To get an intuition on the minimization of this quantity, consider the extreme case where the integral of the square is zero. Then κ' is zero, so κ is constant, and hence the torsion θ' is zero. Thus, the curve is a circle. The isometry property,

$$\left(\int_0^1 [(\kappa_1[x](t) - \kappa_1[y](t))^2 + (\kappa_2[x](t) - \kappa_2[y](t))^2] dt \right)^{1/2} = \|\Phi[x] - \Phi[y]\|_{L^2} = \|x - y\|,$$

indicates that relative square curvatures are preserved by this transformation. Therefore, “centering” data around an example allows us to interpret the total curvature and maximum curvature as lower and upper bounds on the distance from the example in the data space.

For the provided visualizations, the filaments plots are produced by a simple numerical integration strategy coupled with Rodrigues’s formula for exponentiation of a skew-symmetric matrix.

5.1 Boston dataset visualizations

The Boston Housing dataset ([Harrison Jr and Rubinfeld, 1978](#)) provides a 13-dimensional example with a single regression price (median house price in a given statistical area). Figures 8 and 9 consider labeling this dataset according to the decile of the median house price over the dataset. The 2D plots prove difficult to read, but the filament plot visually separates individual points while retaining the expected cluster structure.

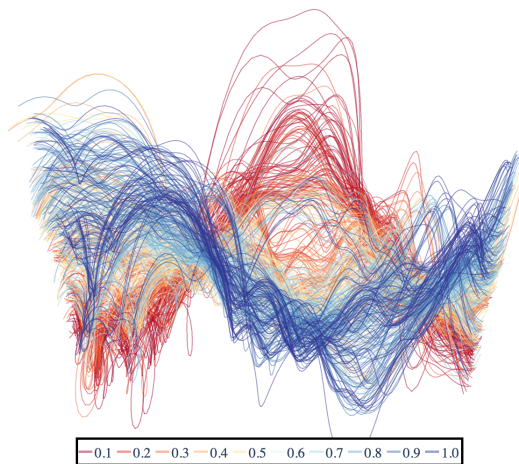


Figure 8: The graphs of the 2D Andrew's plots for the Boston dataset. Deciles of the median house price provide are used to color the different filaments.

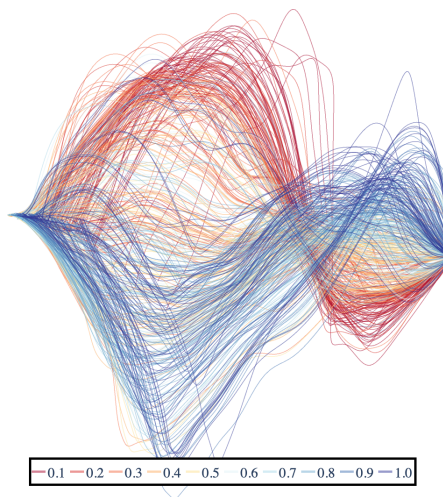


Figure 9: The Filament plot for the Boston housing dataset.

5.2 Breast cancer dataset visualizations

Next, we consider the version of the Wisconsin breast cancer dataset ([Street et al., 1993](#)) provided in the python sklearn package. This dataset has 30 dimension and two classes. In

contrast to the 2D Andrew’s plots in Figure 10, the filament plot in Figure 11 illustrates that the classes are mostly separable with some notable exceptions.

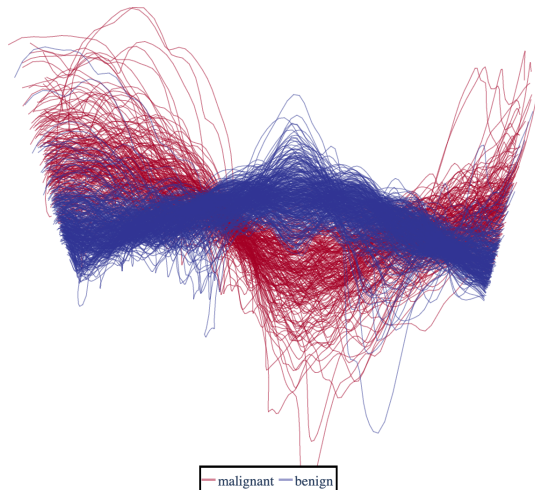


Figure 10: The graphs of the 2D Andrew’s plots for the Wisconsin breast cancer dataset.

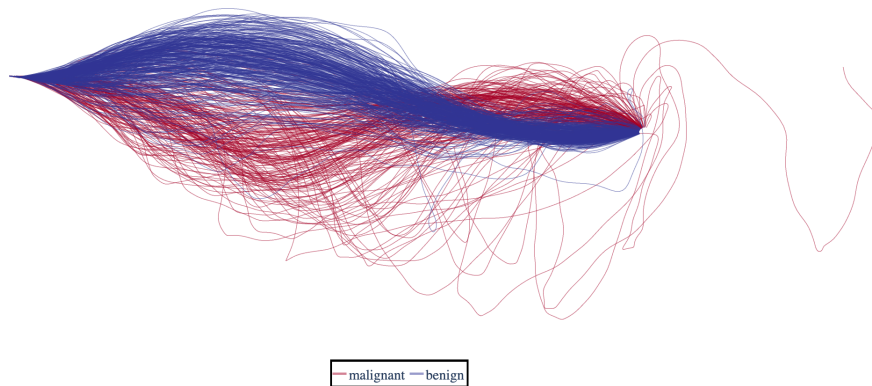


Figure 11: The Filament plot for the Wisconsin breast cancer dataset.

5.3 Digits dataset visualizations

Our last example is 64 dimensional space (Xu et al., 1992). While the logic of visualizing image datasets seems tortured, images only admit small-multiple comparisons, so scatter-plots provide the ability to compare proximity across a larger slice of these dataset. The 2D Andrew’s plots in Figure 12 are quite difficult to read, but the filament plot in Figure 13 separates the data nicely while indicating the proximity of similar classes (for example, 4, 7, and 9 have interesting overlapping structure).

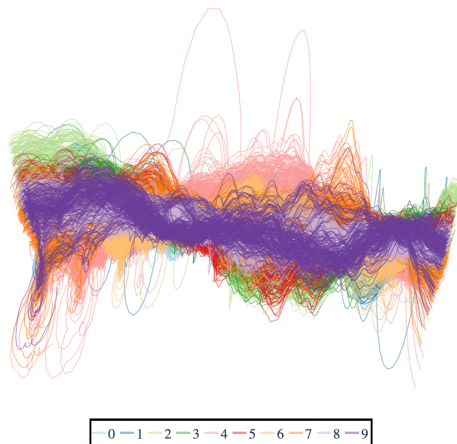


Figure 12: The graphs of the 2D Andrew's plots for the digits dataset.

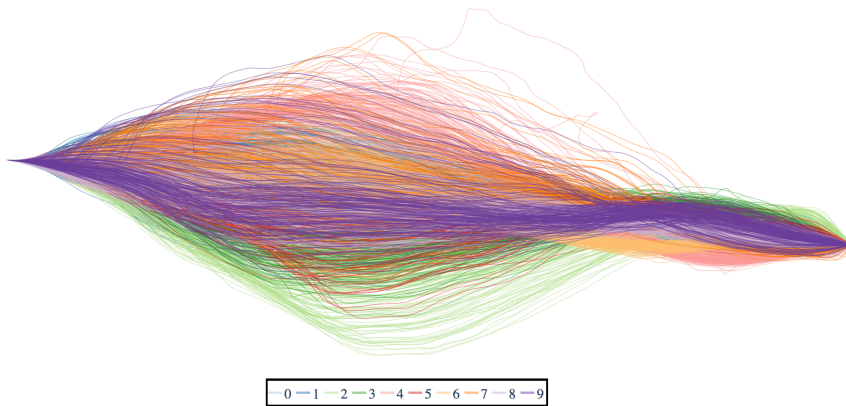


Figure 13: The Filament plot for the digits dataset.

6. Conclusion and discussion

L^1 and L^∞ gap. While the L^1 and L^∞ bounds provide useful visual heuristics, the gap between these bounds grows like \sqrt{d} for our embeddings. This follows from various resolutions of the Littlewood conjecture (Trigub, 2003) in the L^1 case and Erdos (Erdős, 1962) indicates the sharpness of the result in the L^∞ case. We leave it as an open problem to construct embeddings which shrink this gap (perhaps trading off smoothness). Additionally, we leave it as an open problem to construct data embeddings into curves that result in comparison bounds in the Hausdorff metric.

Embeddings of metric spaces into L^∞ . The \sqrt{d} gap mentioned above and the result of (Matoušek, 1990) on $O(N^{2/d} \log^{3/2}(N))$ -distortion embeddings of N -point metric spaces into \mathbb{R}^d suggests that N point metric spaces may be embedded into spaces of functions with a L^1 - L^∞ gap on the order of $O(\log^{5/4}(N))$. (Linial et al., 1995) indicates that certain expander graphs cannot embed without $\Omega(\log(N))$ distortion for ℓ_p^d with $1 \leq p \leq 2$ no matter the dimension of the target space. However, the same paper indicates in Lemma 3.1 that we can embed any finite metric space on N points into ℓ_∞^N . This suggests that we

may embed into spaces of curves under the Hausdorff or L^∞ distance with no distortion, but possibly at the cost of smoothness.

On the other hand, work such as (Bădoiu et al., 2005; Matoušek and Sidiropoulos, 2010) indicates that many of these low-distortion embeddings are difficult to compute. The method we present only requires an SVD and simple numerical integration.

Closed curve problem. Because the linear component of a space curve exhibits the most visual impact, the removal of this component generally reduces biases that would appear in visualizations. Thus, it is interesting to consider embeddings into spaces of closed curves. This may be done by simply taking the image of a periodic curve, but if our goal is to embed into curvatures that induce closed curves, we must confront the *closed curve problem*.

The closed curve problem seeks necessary and sufficient conditions on the curvature (and torsion) functions for closed curves. While (Arroyo et al., 2008) resolves the problem for plane curves in many cases, it is generally agreed that the problem presents a substantial challenge for the case of closed space curves.

References

- Edgar Anderson. The species problem in iris. *Annals of the Missouri Botanical Garden*, 23(3):457–509, 1936.
- David F Andrews. Plots of high-dimensional data. *Biometrics*, pages 125–136, 1972.
- Josu Arroyo, Oscar J Garay, and José J Mencía. When is a periodic function the curvature of a closed plane curve? *The American Mathematical Monthly*, 115(5):405–414, 2008.
- Daniel Asimov. The grand tour: a tool for viewing multidimensional data. *SIAM journal on scientific and statistical computing*, 6(1):128–143, 1985.
- Richard A Becker and William S Cleveland. Brushing scatterplots. *Technometrics*, 29(2):127–142, 1987.
- Bruce C Berndt, Ronald J Evans, and Kenneth S Williams. *Gauss and Jacobi sums*, volume 1. Wiley New York, 1998.
- Jean Bourgain and Mei-Chu Chang. A gauss sum estimate in arbitrary finite fields. *Comptes Rendus Mathématique*, 342(9):643–646, 2006.
- Matthew Brand and Kun Huang. A unifying theorem for spectral embedding and clustering. In *International Workshop on Artificial Intelligence and Statistics*, pages 41–48. PMLR, 2003.
- Mihai Bădoiu, Julia Chuzhoy, Piotr Indyk, and Anastasios Sidiropoulos. Low-distortion embeddings of general metrics into the line. In *Proceedings of the thirty-seventh annual ACM symposium on Theory of computing*, pages 225–233, 2005.
- Kun Chen, Kehui Chen, Hans-Georg Müller, and Jane-Ling Wang. Stringing high-dimensional data for functional analysis. *Journal of the American Statistical Association*, 106(493):275–284, 2011.

- Dianne Cook, Andreas Buja, Javier Cabrera, and Catherine Hurley. Grand tour and projection pursuit. *Journal of Computational and Graphical Statistics*, 4(3):155–172, 1995.
- E Coutsias and N Kazarinoff. The approximate functional formula for the theta function and diophantine gauss sums. *Transactions of the American Mathematical Society*, 350(2):615–641, 1998.
- Emek Demirci Akarsu and Jens Marklof. The value distribution of incomplete gauss sums. *Mathematika*, 59(2):381–398, 2013.
- Paul Embrechts and Agnes M Herzberg. Variations of andrews’ plots. *International Statistical Review/Revue Internationale de Statistique*, pages 175–194, 1991.
- John W Emerson, Walton A Green, Barret Schloerke, Jason Crowley, Dianne Cook, Heike Hofmann, and Hadley Wickham. The generalized pairs plot. *Journal of Computational and Graphical Statistics*, 22(1):79–91, 2013.
- P Erdős. An inequality for the maximum of trigonometric polynomials. In *Annales Polonici Mathematici*, volume 2, pages 151–154, 1962.
- Jerome H Friedman and John W Tukey. A projection pursuit algorithm for exploratory data analysis. *IEEE Transactions on computers*, 100(9):881–890, 1974.
- César Garcia-Osorio and Colin Fyfe. An extension of grand tour methods based on andrews curves. 2004.
- César Garcia-Osorio and Colin Fyfe. Visualization of high-dimensional data via orthogonal curves. *Journal of Universal Computer Science*, 11(11):1806–1819, 2005.
- Vivek K Goyal, Jelena Kovačević, and Jonathan A Kelner. Quantized frame expansions with erasures. *Applied and Computational Harmonic Analysis*, 10(3):203–233, 2001.
- Godfrey Harold Hardy, John Edensor Littlewood, et al. Some problems of diophantine approximation: Part ii. the trigonometrical series associated with the elliptic ϑ -functions. *Acta mathematica*, 37:193–239, 1914.
- David Harrison Jr and Daniel L Rubinfeld. Hedonic housing prices and the demand for clean air. *Journal of environmental economics and management*, 5(1):81–102, 1978.
- John A Hartigan. Printer graphics for clustering. *Journal of Statistical Computation and Simulation*, 4(3):187–213, 1975.
- Alfred Inselberg. The plane with parallel coordinates. *The visual computer*, 1(2):69–91, 1985.
- Henryk Iwaniec and Emmanuel Kowalski. *Analytic number theory*, volume 53. American Mathematical Soc., 2004.
- Ravindra Khattree and Dayanand N Naik. Andrews plots for multivariate data: some new suggestions and applications. *Journal of statistical planning and inference*, 100(2):411–425, 2002.

- JA Koziol and Werner Hacke. A bivariate version of andrews plots. *IEEE transactions on biomedical engineering*, 38(12):1271–1274, 1991.
- Joseph B Kruskal. *Multidimensional scaling*. Number 11. Sage, 1978.
- Derrick Henry Lehmer. Incomplete gauss sums. *Mathematika*, 23(2):125–135, 1976.
- Nathan Linial, Eran London, and Yuri Rabinovich. The geometry of graphs and some of its algorithmic applications. *Combinatorica*, 15(2):215–245, 1995.
- Jiří Matoušek. Bi-lipschitz embeddings into low-dimensional euclidean spaces. *Commentationes Mathematicae Universitatis Carolinae*, 31(3):589–600, 1990.
- Jiří Matoušek and Anastasios Sidiropoulos. Inapproximability for metric embeddings into \mathbb{R}^d . *Transactions of the American Mathematical Society*, 362(12):6341–6365, 2010.
- Leland McInnes, John Healy, Nathaniel Saul, and Lukas Großberger. Umap: Uniform manifold approximation and projection. *Journal of Open Source Software*, 3(29):861, 2018.
- Rida E Moustafa. Andrews curves. *Wiley Interdisciplinary Reviews: Computational Statistics*, 3(4):373–382, 2011.
- Mram Murty and Siddhi Pathak. Evaluation of the quadratic gauss sum. *Evaluation*, 86(1-2), 2017.
- Frank Olver. *Asymptotics and special functions*. CRC Press, 1997.
- Frank WJ Olver, Daniel W Lozier, Ronald F Boisvert, and Charles W Clark. *NIST handbook of mathematical functions hardback and CD-ROM*. Cambridge university press, 2010.
- KI Oskolkov. On functional properties of incomplete gaussian sums. *Canadian Journal of Mathematics*, 43(1):182–212, 1991.
- RB Paris. An asymptotic expansion for the generalised quadratic gauss sum revisited. *Journal of Classical Analysis*, 5(1):15–24, 2014.
- W Nick Street, William H Wolberg, and Olvi L Mangasarian. Nuclear feature extraction for breast tumor diagnosis. In *Biomedical image processing and biomedical visualization*, volume 1905, pages 861–870. International Society for Optics and Photonics, 1993.
- Roald Mikhailovich Trigub. A lower bound for the l^1 -norm of Fourier series of polynomial type. *Mathematical notes*, 73(5):900–903, 2003.
- Edward R Tufte, Nora Hillman Goeler, and Richard Benson. *Envisioning information*, volume 2. Graphics press Cheshire, CT, 1990.
- PA Tukey and JW Tukey. Graphical display of data sets in 3 or more dimensions. *Interpreting multivariate data*, 189:275, 1981.
- Laurens Van der Maaten and Geoffrey Hinton. Visualizing data using t-sne. *Journal of machine learning research*, 9(11), 2008.

Georg Von Mayr. *Die gesetzmässigkeit im gesellschaftsleben*, volume 23. De Gruyter Oldenbourg, 1877.

Edward J Wegman and Ji Shen. Three-dimensional andrews plots and the grand tour. *Computing Science and Statistics*, pages 284–284, 1993.

Lei Xu, Adam Krzyzak, and Ching Y Suen. Methods of combining multiple classifiers and their applications to handwriting recognition. *IEEE transactions on systems, man, and cybernetics*, 22(3):418–435, 1992.